JOURNAL OF GEOPHYSICAL RESEARCH: ATMOSPHERES, VOL. 118, 7024–7045, doi:10.1002/jgrd.50565, 2013

The relative roles of upper and lower tropospheric thermal contrasts and tropical influences in driving Asian summer monsoons

Aiguo Dai,[1,2] Hongmei Li,[3] Ying Sun,[4] Li-Ciao Hong,[5] Lin Ho,[5] Chia Chou,[5,6] and Tianjun Zhou[7]

Received 15 March 2013; revised 16 May 2013; accepted 7 June 2013; published 9 July 2013.

[1] Summer thermal structure and winds over Asia show a larger land-ocean thermal gradient in the upper than in the lower troposphere, implying a bigger role of the upper troposphere in driving the Asian summer monsoon circulation. Using data from atmospheric re-analyses and model simulations, we show that the land-ocean thermal contrast in the mid-upper (200–500 hPa) troposphere (TCupper) contributes about three times as much as the thermal contrast in the mid-lower (500–850 hPa) troposphere (TClower) in determining both the strength and variations of Asian summer monsoon circulations. Tropical sea surface temperature anomalies associated with the annual cycle, El Niño-Southern Oscillation, decadal changes, and global warming all are accompanied with much larger variations and changes in TCupper than in TClower, partly due to enhanced latent heating aloft from convection. The variations and changes in TCupper and TClower are highly correlated with the strength of the South Asian Summer Monsoon (SASM) and the East Asian Summer Monsoon (EASM) in their respective sectors during the past 50–60 years. In particular, the weakening of the EASM since the 1950s is caused by the weakening mainly in TCupper and secondarily in TClower induced mainly by recent tropical surface warming, although spurious cooling over East Asia seen in reanalysis data may have enhanced this weakening. However, the strength of the SASM and EASM monsoons follows TCupper but decouples with TClower in the global warming case in the 21st century. The results suggest that the TCupper plays a dominant role and provides an efficient mechanism through which tropical oceans can influence extratropical monsoons.

Citation: Dai, A., H. Li, Y. Sun, L.-C. Hong, L. Ho, C. Chou, and T. Zhou (2013), The relative roles of upper and lower tropospheric thermal contrasts and tropical influences in driving Asian summer monsoons, *J. Geophys. Res. Atmos.*, *118*, 7024–7045, doi:10.1002/jgrd.50565.

1. Introduction

[2] A basic driver of the Asian monsoons is the differential heating by the Sun over the Asian continent and the ocean to the south and east, which creates atmospheric temperature and pressure gradients that initiate and largely drive the monsoon circulation [*Webster*, 1987; *Zeng and Li*, 2002; *Holton*, 2004; *He et al*., 2007]. However, classical land-ocean contrast models with surface temperature gradients can only generate a shallow circulation [*Schneider and Lindzen*, 1977] and cannot explain the deep vertical structure of the South Asian Summer Monsoon (SASM). Deep tropospheric heating (e.g., from moist convection) is required for the deep SASM circulation, and it may be represented by the meridional temperature gradient in the free troposphere [*Webster et al*., 1998; *Goswami and Xavier*, 2005]. Despite these findings, previous studies have used different definitions of land-ocean thermal contrasts to study SASM variations, such as the land-ocean difference of near-surface temperature [*Fu and Fletcher*, 1985], 200–500 hPa thickness [*Li and Yanai*, 1996; *Kawamura*, 1998; *Chou*, 2003], 200–1000 hPa thickness [*Holton*, 2004, p.380], and the net energy input into the atmosphere [*Chou and Neelin*, 2003]. These studies have shown that the thermal difference at different levels between the Asian continent, especially the Tibetan Plateau (TP), and the tropical oceans to the south, is closely linked to the establishment, seasonal evolution, and interannual to interdecadal variations of the SASM. These studies all show a positive

[1]Department of Atmospheric and Environmental Sciences, State University of New York at Albany, Albany, New York, USA.
[2]National Center for Atmospheric Research, Boulder, Colorado, USA.
[3]Max Planck Institute of Meteorology, Hamburg, Germany.
[4]National Climate Center, China Meterological Administration, Beijing, China.
[5]Department of Atmospheric Sciences, National Taiwan University, Taipei, Taiwan.
[6]Research Center for Environmental Changes, Academia Sinica, Taipei, Taiwan.
[7]LASG, Institute of Atmospheric Physics, Chinese Academy of Sciences, Beijing, China.

Corresponding author: A. Dai, Department of Atmospheric and Environmental Sciences, State University of New York at Albany, 1400 Washington Ave., Albany, NY 12222, USA. (adai@albany.edu)

2169-897X/13/10.1002/jgrd.50565

correlation between the SASM intensity and the thermal contrast at different levels in historical records, as expected from the thermal wind relationship [*Holton*, 2004].

[3] However, a recent analysis by *Sun et al*. [2010] shows that the SASM intensity decreases together with the mid-upper tropospheric (200–500 hPa) thermal contrast, while the surface and lower-tropospheric thermal contrasts increase in model-predicted 21st century climate under increased greenhouse gases (GHGs). These findings suggest that the land-ocean thermal contrasts in the upper and lower troposphere can behave differently in certain cases, and that it is the thermal contrast in the mid-upper troposphere, not near the surface or in the lower troposphere, that drives the SASM in the model-predicted future climate. For the East Asian Summer Monsoon (EASM), *Sun and Ding* [2011] showed that future changes in 850 hPa meridional wind over East Asia are consistent with changes in the low-level zonal temperature gradient.

[4] Given that latent heating is another major driver of monsoons [*Webster*, 1987; *Holton*, 2004; *He et al*., 2004, 2007] besides the surface-heating induced thermal contrast and that the latent heating from atmospheric convection is concentrated between about 5 and 10 km above the ocean surface at low latitudes [*Yang et al*., 2006], it is not surprising that the land-ocean thermal contrast in the mid-upper troposphere may play a more important role than the thermal contrast near the surface or in the lower troposphere in determining the strength of the SASM and other summer monsoons. Furthermore, as discussed by *Webster* [1987], warm air over land during summer expands upward more than cold air over ocean, resulting in larger land-ocean pressure gradients in the upper than in the lower troposphere. This also implies a bigger role of the upper than the lower troposphere in driving a monsoon circulation. This notion, however, has still not been widely adopted in the literature, as reflected by the use of near-surface or lower-tropospheric thermal contrasts in previous studies [e.g., *Fu and Fletcher*, 1985; *Bhaskaran*, 2012] and the fact that many monsoon indices for the EASM are based on low-level winds or sea-level pressure (SLP) only [*Wang et al*., 2008].

[5] The importance of the land-ocean thermal contrast within the whole troposphere in driving the deep monsoon circulation has been recognized previously [e.g., *Schneider and Lindzen*, 1977; *Webster et al*., 1998; *Goswami and Xavier*, 2005], and many studies have shown that the upper tropospheric thermal (and the associated pressure) gradient plays an important role in driving the SASM [*Webster*, 1987] and its onset and interannual variations [e.g., *Yanai and Li*, 1994; *Li and Yanai*, 1996; *Kawamura*, 1998; *He et al*., 2003], as well as for the EASM [*Zhang et al*., 2006; *Chen et al*., 2010]. The land-ocean thermal contrast for the EASM is, however, more complex than that for the SASM, with the zonal gradient between the Indochina Peninsula and the nearby seas in the Bay of Bengal and the South China Sea during spring and between East China and the North Pacific during summer being also important besides the south-north gradient [*Ding and Chan*, 2005; *He et al*., 2007]. The warm air over the TP is advected to over East China which enhances the summer land-sea thermal contrasts between East Asia and the oceans to the south and east, and the monsoon rainfall over East Asia further enhances the land-ocean thermal contrasts [*Duan and Wu*, 2005].

[6] In this study, we further quantify the *relative roles* of the thermal contrasts in the mid-upper (200–500 hPa) and mid-lower (500–850 hPa) troposphere in driving both SASM and EASM circulations by examining their relationships on seasonal to multidecadal time scales, and apply the results to propose a mechanism through which remote tropical sea surface temperature (SST) variations can effectively influence Asian monsoons and to analyze historical and model-projected future Asian monsoon changes. Although previous studies [e.g., *Zhou et al*., 2009b; *Li et al*., 2010] have analyzed the historical changes in Asian summer monsoons, few studies have done systematic analyses of monsoon changes in the context of the thermal contrast changes. Our results reinforce the view that the land-ocean thermal contrasts in the whole troposphere, especially in the mid-upper troposphere where latent heating from deep convection is largest, determine the circulation strength and variations of the SASM and EASM; whereas land-ocean thermal contrasts near the surface and in the mid-lower troposphere often play a smaller role.

[7] We realize that latent heating from monsoon rainfall can affect the land-sea thermal contrast, thus providing a strong positive feedback for the monsoon circulation. From the perspective of the thermal wind relation, however, it is the land-sea temperature gradient, regardless of its causes, that determines the vertical wind shear that is often used as a measure of the monsoon circulation strength. Here we focus on the tropospheric land-sea thermal contrasts and their relationship with the monsoon circulation intensity, with only brief discussion of the causes of the thermal gradients (section 5). Furthermore, the wind-shear-based monsoon indices used here are a measure of the monsoon circulation intensity only; other monsoon characteristics such as monsoon rainfall are not discussed here. The SASM and EASM also have different characteristics in terms of their land-sea thermal contrasts; however, our results show a common feature among them in the coupling strength between the monsoon circulation intensity and the thermal contrasts in the lower and upper troposphere.

2. Definition of Monsoon Indices and Thermal Contrasts

2.1. Common Monsoon Indices

[8] Various monsoon indices have been used to measure the strength of Asian monsoons, especially for the EASM [*Wang et al*., 2008], for which the zonal land-sea gradient in SLP [*Guo*, 1983; *Zhou et al*., 2009b] is often used in the EASM community. For the SASM, the 850–200 hPa wind shear used by *Webster and Yang* [1992] is a popular index, because it is directly linked to the land-ocean thermal contrasts through the thermal wind equations (see Appendix A). *Wang et al*. [2008] showed that, even for the EASM, the wind-shear-based indices are among the better performing ones for measuring EASM's intensity. Here we adopted this index because of its close link to the thermal contrast in the whole free troposphere and also because of our focus on both the lower and upper branches of a monsoon circulation.

[9] *Webster and Yang* [1992] defined a SASM index (SASMI) as the zonal wind difference between 850 hPa and 200 hPa ($U_{850} - U_{200}$) averaged over approximately 0°–20° N and 60°–110°E (Figure 1). This SASMI reflects the combined strength in both the lower- and upper-level winds within a monsoon circulation; thus, it provides a more complete depiction than using low-level winds (e.g., U_{850}) alone. Because ($-U_{200}$) is larger than U_{850} over Asia, the SASMI

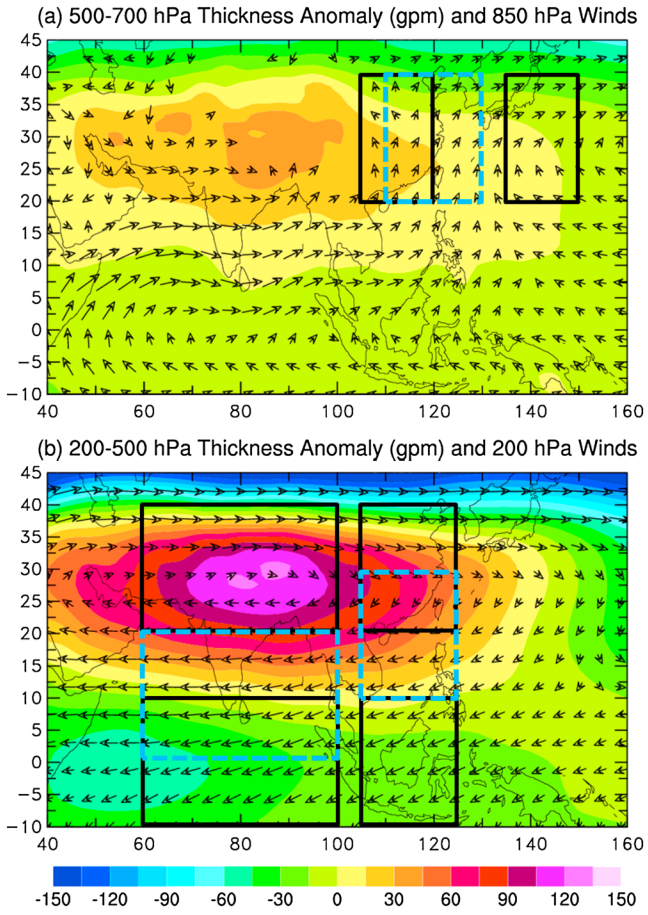

Figure 1. (a) Long-term (1971–2000) mean of JJA 500–700 hPa thickness anomalies (relative to the mean of the whole domain, colors, in gpm) and 850 hPa winds (arrows, the longest arrows are for 18.8 m s^{-1}) from ERA-40 reanalysis. (b) Same as Figure 1a but for 200–500 hPa thickness anomalies and 200 hPa winds (the longest arrows are for 32.6 m s^{-1}). The rectangular boxes with solid lines in Figure 1b indicate the averaging areas for the south-north thermal contrasts (solid line) for SASM (60°–100°E) and EASM (105°–125°E), while the rectangular boxes with dashed blue lines denote the areas over which the SASMI and EASMIu are averaged. The boxes in Figure 1a are for the west-east contrast and EASMIv averaging areas. The thickness anomalies for 500–850 hPa are similar to Figure 1a over areas outside the Tibetan Plateau.

is often influenced more by U_{200} than U_{850} [*Webster et al.*, 1998; *Wang et al.*, 2008]. Thus, a SASMI change may not reflect changes in low-level monsoon winds, which are the focus of many studies on the EASM [*Wang et al.*, 2008]. However, as shown in Figures 1–3 the U_{850} is non-negligible compared with the U_{200} over the SASM and EASM sectors, and the V component is comparable at the two levels over the EASM sector. Thus, the wind-shear-based monsoon indices used in this paper include significant contributions from the low-level winds. We will examine both U_{850} and U_{200} when the wind-shear-based index shows a long-term trend.

2.2. Link to Thermal Gradients

[10] From equation (A1) in Appendix A, the SASMI is linked to the south-north gradient of the geopotential difference: SASMI $\equiv U_{850} - U_{200} = \frac{1}{f}\frac{\partial}{\partial y}(\Phi_{200} - \Phi_{850}) = \frac{1}{f}\frac{\partial}{\partial y}(\Phi_{200} - \Phi_{500}) + \frac{1}{f}\frac{\partial}{\partial y}(\Phi_{500} - \Phi_{850}) \equiv \frac{g_o}{f}$ (TCupper + TClower). Here we define the mid-upper tropospheric south-north thermal contrast (TCupper) as $\frac{\partial}{\partial y}(Z_{200} - Z_{500})$ and the mid-lower tropospheric south-north thermal contrast (TClower) as $\frac{\partial}{\partial y}(Z_{500} - Z_{850})$. Here Φ_x and Z_x denote the geopotential and geopotential height at a given level x, respectively. The climatological winds over South Asia at the 200, 500, and 850 hPa levels (Figures 1 and 2) imply that the mean TCupper $\left[= \frac{f}{g_o}(U_{500} - U_{200})\right]$ should be larger than the mean TClower $\left[= \frac{f}{g_o}(U_{850} - U_{500})\right]$, as $(-U_{200})$ is considerably larger than U_{500} and U_{850}, both of which are positive over 60°–100°E and 0°–20°N. The layer thickness for the upper and lower troposphere over the Asian sector (Figure 1) confirms that the mean TCupper is larger than TClower, as it should be based on thermal wind relation. Thus, one should expect a bigger role by the upper troposphere than the lower troposphere in driving the mean summer monsoon circulation for both SASM and EASM. Despite this, the notion that the TCupper dominates over TClower for SASM (and EASM) circulations is still not well accepted in the literature.

[11] A TCupper with a larger mean does not necessarily warrant a bigger role in explaining *variations and long-term changes* in the SASM and EASM, because it is the changes and variations in TCupper and TClower that matter. Here we quantify the variations and changes in the TCupper and TClower to examine their contributions to the variance of the SASM and EASM.

[12] Although we found that TCupper and its variations play a bigger role than TClower for driving the SASM and EASM circulations and their variations and changes, the lower troposphere is important in the sense that it can affect TCupper by providing moisture and sensible heat fluxes to the upper troposphere. Here we emphasize the role of TCupper mainly to correct the notion that Asian summer monsoons (especially EASM) are controlled by land-ocean temperature differences near the surface or in the lower troposphere, as this thinking is incorrect and causes an apparent paradox in interpreting model-projected future monsoon changes [*Sun et al.*, 2010; *Bhaskaran*, 2012].

2.3. Monsoon Indices and Thermal Contrasts Used in This Study

[13] To estimate the south-north gradient, the geopotential height thickness is first averaged over the rectangular boxes with solid lines in Figure 1 and then the north-minus-south box-mean values are used as the south-north contrast for comparison with the SAMSI averaged over the rectangular box with dashed lines and located between the two boxes with solid lines (Figure 1). That is, for the SASM,

$$\begin{aligned}\text{TCupper} \approx\ & Z(200-500\ \text{hPa}, 60°-100°\text{E}, 20°-40°\text{N}) \\ & -Z(200-500\ \text{hPa}, 60°-100°\text{E}, 10°\text{S}-10°\text{N})\end{aligned}$$

$$\begin{aligned}\text{TClower} \approx\ & Z(500-700\ \text{hPa}, 60°\text{E}-100°\text{E}, 20°\text{N}-40°\text{N}) \\ & -Z(500-700\ \text{hPa}, 60°\text{E}-100\text{E}, 10°\text{S}-10°\text{N})\end{aligned}$$

$$\begin{aligned}\text{SASMI} =\ & \text{U}(850\ \text{hPa}, 60°-100°\text{E}, 0°-20°\text{N}) \\ & -\text{U}(200\ \text{hPa}, 60°-100\text{E}, 0°-20°\text{N}).\end{aligned}$$

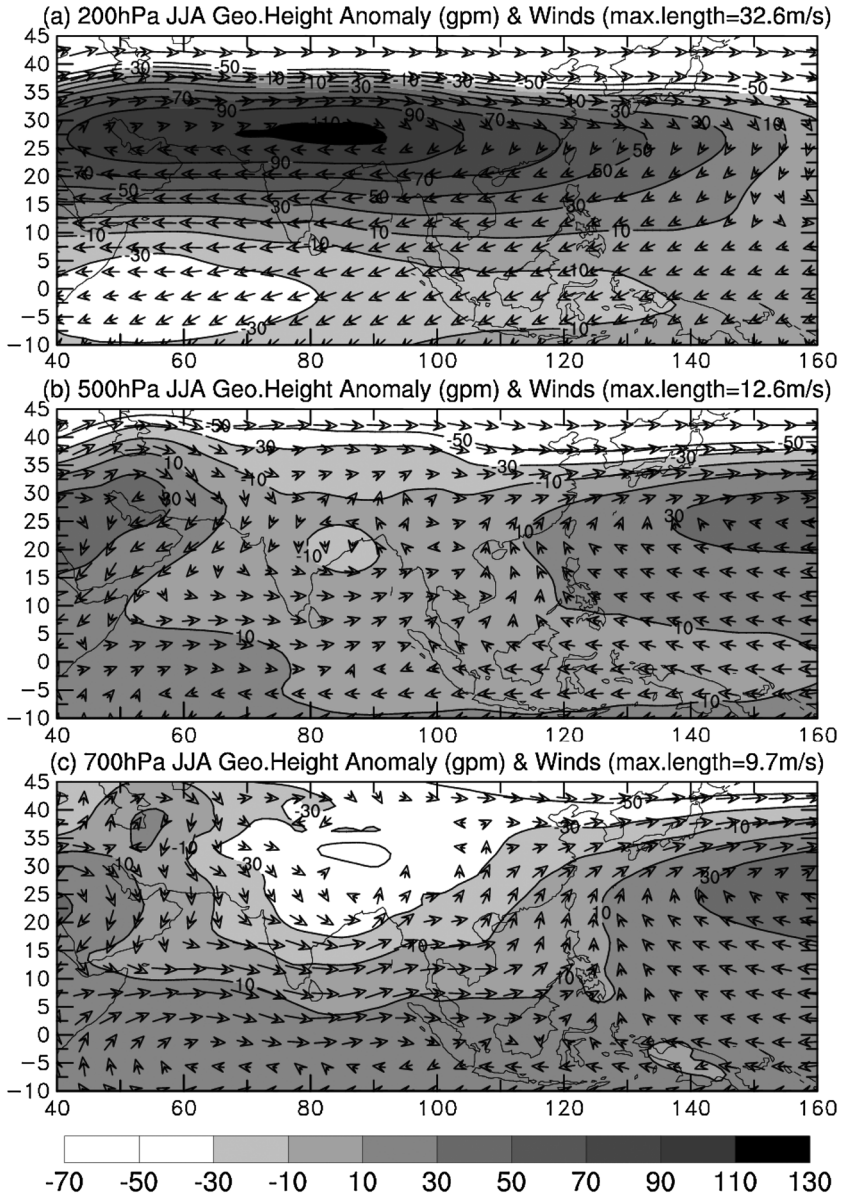

Figure 2. Long-term (1971–2000) mean of JJA geopotential height anomalies (shading in gpm, relative to the mean of the whole domain) and winds (arrows) at (a) 200, (b) 500, and (c) 700 hPa based on ERA-40 reanalysis for the Asian domain (40°–160°E and 10°S–45°N).

[14] For the EASM, the south-north contrasts and zonal wind index are defined as:

$$\mathrm{TCupper} \approx Z(200-500\ \mathrm{hPa}, 105^\circ-125^\circ\mathrm{E}, 20^\circ-40^\circ\mathrm{N}) - Z(200-500\ \mathrm{hPa}, 105^\circ-125^\circ\mathrm{E}, 10^\circ\mathrm{S}-10^\circ\mathrm{N})$$

$$\mathrm{TClower} \approx Z(500-850\ \mathrm{hPa}, 105^\circ-125^\circ\mathrm{E}, 20^\circ-40^\circ\mathrm{N}) - Z(500-850\ \mathrm{hPa}, 105^\circ-125^\circ\mathrm{E}, 10^\circ\mathrm{S}-10^\circ\mathrm{N})$$

$$\mathrm{EASMIu} = \mathrm{U}(850\ \mathrm{hPa}, 105^\circ-125^\circ\mathrm{E}, 10^\circ-30^\circ\mathrm{N}) - \mathrm{U}(200\ \mathrm{hPa}, 105^\circ-125^\circ\mathrm{E}, 10^\circ-30^\circ\mathrm{N}),$$

and the west-east contrasts and meridional wind index, which are important for the EASM, are defined as

$$\mathrm{TEupper} \approx \mathrm{Z}(200-500\ \mathrm{hPa}, 105^\circ-120^\circ\mathrm{E}, 20-40^\circ\mathrm{N}) - Z(200-500\ \mathrm{hPa}, 135^\circ-150^\circ\mathrm{E}, 20^\circ-40^\circ\mathrm{N})$$

$$\mathrm{TElower} \approx \mathrm{Z}(500-850\ \mathrm{hPa}, 105^\circ-120^\circ\mathrm{E}, 20^\circ-40^\circ\mathrm{N}) - \mathrm{Z}(500-850\ \mathrm{hPa}, 135^\circ-150^\circ\mathrm{E}, 20^\circ-40^\circ\mathrm{N})$$

$$\mathrm{EASMIv} = \mathrm{V}(850\ \mathrm{hPa}, 110^\circ-130^\circ\mathrm{E}, 20^\circ-40^\circ\mathrm{N}) - \mathrm{V}(200\ \mathrm{hPa}, 110^\circ-130^\circ\mathrm{E}, 20^\circ-40^\circ\mathrm{N}).$$

[15] For SASM, we will only examine the south-north gradient and the zonal wind following most previous studies [e.g., *Webster and Yang*, 1992; *Wang et al*., 2008], although the thermal gradient in the west-east direction was also found to be important for the monsoon rainfall in southern India and the Bay of Bengal [*Kucharski et al*., 2011].

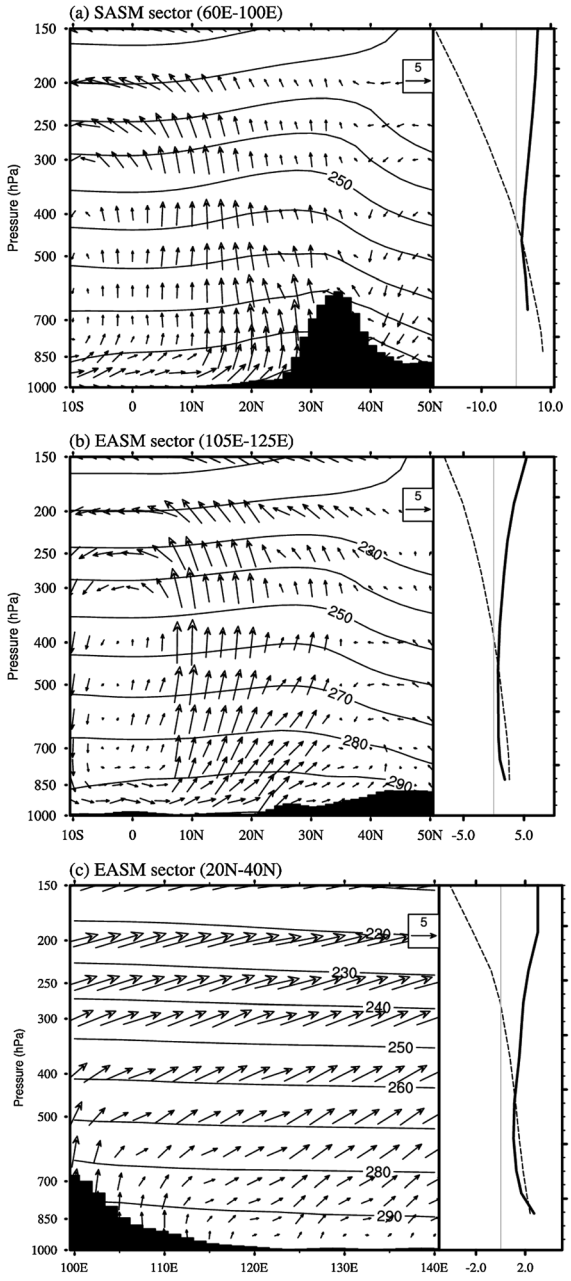

Figure 3. (a) (left panel) Latitude-height cross section of long-term (1971–2000) mean of JJA temperature (contours, K) and winds (arrows, m s^{-1}) averaged over the SASM sector (60°–100°E), and (right panel) vertical profiles of the mean zonal wind component U (dashed line, m s^{-1}) averaged over (0°–20°N, 60°–110°E) and the north (20°–40°N, 60°–100°E) minus south (10°S–10°N, 60°–100°E) temperature difference (solid line, K) from ERA-40. (b) Same as Figure 3a but for the EASM sector (105°–125°E) and the U is averaged over (10°–30°N, 105°–125°E). (c) Same as Figure 3a but for longitude-height cross section averaged over 20°–40°N and the vertical profiles are for the mean meridional wind component V (dashed line, m s^{-1}) averaged over (20°–40°N, 110°N–130°E) and the west (20°–40°N, 105°–120°E) minus east (20°–40°N, 135°–150°E) temperature difference (solid line, K). See Figure 1 for the averaging the boxes. The black areas are the sector-averaged mean terrain.

[16] Our EASMIu is very similar to that used by *Webster and Yang* [1992], which is the fifth EASM index listed in Table 1 of *Wang et al*. [2008]. Also, the above TCupper for SASM is very similar to the monsoon index used by *Kawamura* [1998]. The EASMIv, TEupper, and TElower are analogues to the EASMIu, TCupper, and TClower, but are based on the thermal wind equation for the meridional wind component (equation (A2) in Appendix A). Thus, they have the same theoretical consideration as for EASMIu, TCupper, and TClower. To our knowledge, they have not been used in the literature, although 850 hPa v winds and east-west gradients of SLP, surface temperature, and 500 hPa geopotential have been used previously to quantify the EASM [*Wang et al*., 2008; *Sun and Ding*, 2011]. One major difference between the EASM and SASM is that the EASM is influenced by the land-sea thermal contrasts in both the south-north and west-east directions. Thus, we use both EASMIu (TCupper and TClower) and EASMIv (TEupper and TElower) to quantify the EASM. These two components (and their thermal contrasts) are independent to each other, although the vector winds over East Asia will be influenced by both of them.

[17] Note that we used 500–700 hPa thickness for TClower for the SASM case since the mean surface for the TP (60°–100°E, 20°–40°N) is around 700 hPa and the thickness anomalies (relative to the domain mean) (Figure 1) are very similar outside the TP between the 500–700 hPa and 500–850 hPa cases. We chose 105°–125°E as the EASM longitudinal sector, but results for a wider sector (e.g., 110°–140°E) were similar. For TEupper and TElower, we used the west-minus-east thickness difference, so that they are positively related to EASMIv according to equation (A2) in Appendix A. Also, we did not include the TP region explicitly in the thermal contrast definitions for the EASM, since the TP is west of the EASM domain and above the lower branch of the EASM circulation. However, the elevated heating over the TP affects the temperature and layer thickness over a much larger region around the TP, including East China (Figure 1); thus, it can still affect the EASM in the above definitions. Tests with slightly different boxes in Figure 1 (e.g., moving the northern boundary from 40°N to 35°N) showed that the results are not sensitive to the definitions of the averaging boxes.

[18] Here we used the layer thickness (ΔZ), instead of the layer-mean temperature $\overline{T}$, in defining the thermal contrasts in the north-south and west-east directions. The ΔZ and $\overline{T}$ differ by a factor: $\Delta Z = \overline{T}\ R/g_o\ [\ln(p_o/p_1)]$, where $\ln(p_o/p_1) = \ln(500/200) = 0.9163$ for the 200–500 hPa layer and $= \ln(850/500) = 0.5306$ for the 500–850 hPa layer (or 0.3365 for the 500–700 hPa layer for the SASM case). Thus, *for the same temperature gradient, the 200–500 hPa layer contributes 73% more than the 500–850 hPa layer to the* $U_{850} - U_{200}$ *wind shear* based on equation (A1), despite the fact that the 500–850 hPa layer is 50 hPa (17%) thicker than the 200–500 hPa layer in terms of air mass. For the SASM case, the 200–500 hPa layer contributes 2.7 times that from the 500–700 hPa layer to the $U_{700} - U_{200}$ wind shear for similar temperature gradients. These estimates illustrate the importance of using ΔZ in computing the land-ocean thermal contrasts and imply that the mid-upper troposphere may play a bigger role in determining the strength of the monsoon circulation. This result is also consistent with the larger land-ocean pressure gradient in the upper than in the lower troposphere

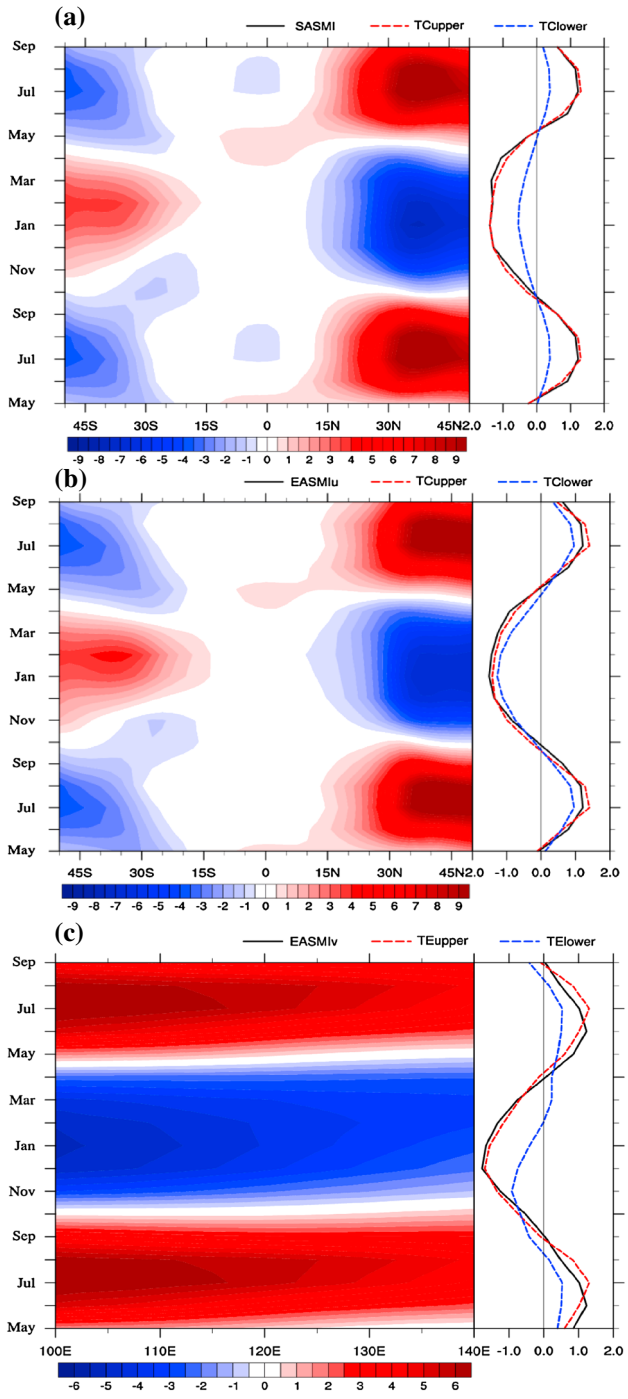

Figure 4. (a) Latitude-month cross section of long-term (1971–2000) mean anomalies (with annual mean removed) of 60°–100°E averaged 200–500 hPa mean temperature (K, left panel) and mean seasonal evolution (right panel) of normalized anomalies (relative to annual mean) of SASMI (black line), TCupper (red) and TClower (blue, normalized with the s.d. of TCupper based on ERA-40. (b) Same as Figure 4a but for the cross section over 105°–125°E and EASMIu (black), TCupper (red), and TClower (blue, normalized with the s.d. of TCupper). (c) Same as Figure 4a but for longitude-month cross section of 200–500 hPa mean temperature (K) averaged over 20°–40°N (left panel) and EASMIv, TEupper, and TElower (right panel). See section 3 for details.

derived based on air's compressibility as a function of temperature by *Webster* [1987].

3. Data and Model Simulations

[19] To compute the SASMI, EASMIu, EASMIv, TCupper, TClower, TEupper, and TElower defined in section 2, we used monthly data of atmospheric temperature, geopotential height, and winds from the ERA-40 (1957-2002 [*Uppala et al*., 2005]) and NCEP/NCAR (1948-present [*Kalnay et al*., 1996]) reanalyses. These reanalysis data were used to quantify the relationship between the monsoon indices and the corresponding thermal contrasts on seasonal, interannual, decadal, and longer time scales, and the relative roles played by the TCupper and TEupper relative to TClower and TElower, respectively. Although the reanalysis data are known to have various biases and inhomogeneity problems [e.g., *Wu et al*., 2005] and thus are best used for examining spatial and short-term (seasonal to multiyear) variations, our focus here is on the relationship between the monsoon indices and the thermal contrasts, not the long-term changes, although decadal changes relevant to the SASM and EASM and common in both reanalyses are also discussed and critically evaluated.

[20] Model ensemble simulations using the NCAR (CAM3) and GFDL (AM2.1) atmospheric general circulation models (AGCMs) forced with observed SSTs from 1950 to 1999 were also analyzed and compared with the reanalysis data. These historical model simulations were described and used in *Li et al*. [2010], who did not analyze tropospheric thermal contrasts. We recognize that SST-forced AGCM runs are best used for examining tropical atmospheric responses to surface forcing, while their usefulness may be limited for mid- and high-latitudes where two-way air-sea interactions are important [*Zhou et al*., 2009c]. To examine the relationship between Asian monsoon indices and their corresponding thermal contrasts under global warming, we also analyzed model data from seven models selected from all the models participated in the IPCC Fourth Assessment Report (AR4) based on their ability in simulating the present-day SASM. We used one simulation from each of the seven models for the 20th century climate under observed GHG and other forcing and the 21st century climate under the A1B (an intermediate) emissions scenario. These simulations are described and used by *Sun et al*. [2010].

4. Results

4.1. Relationship on Seasonal, Interannual, and Decadal Time Scales

[21] In this subsection, we examine the relationship between the monsoon indices (SASMI, EASMIu, EASMIv) and their corresponding thermal contrasts in the mid-upper and mid-lower troposphere on different time scales. From this, we further demonstrate that the thermal contrast in the mid-upper troposphere plays a bigger role than that in the mid-lower troposphere in explaining variations and changes in the monsoon circulation intensity, although the thermal contrasts in the upper and lower troposphere are often positively correlated in historical data.

[22] Atmospheric temperature does not vary much seasonally within about 15°S–15°N, but has a strong annual cycle outside this zone (Figure 4). Thus, the large annual cycle in the thermal contrasts (color lines in Figure 4) results mainly from

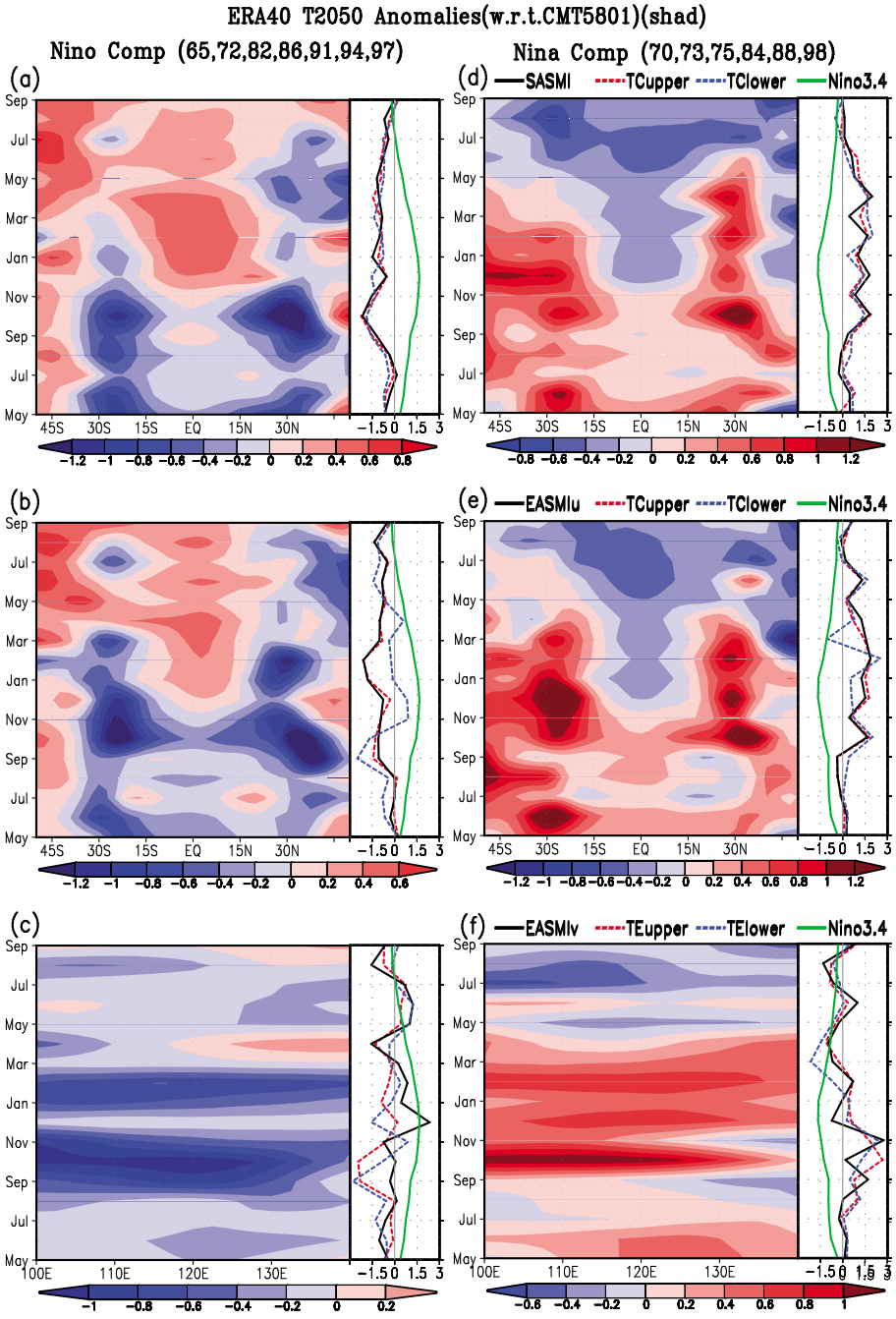

Figure 5. Same as Figure 4 but for departures from the 1958–2001 mean annual cycle during El Niño years (1965, 1972, 1982, 1986, 1991, 1994, and 1997; left column) and La Niña years (1970, 1973, 1975, 1984, 1988, and 1998; right column). Green line is the SST anomaly averaged over the Niño3.4 region (5°S–5°N, 120°–170°W).

seasonal variations over the Asian continent. Furthermore, both the SASMI and EASMIu covary closely with their respective TCupper and TClower during the annual cycle; however, TCupper has a larger seasonal amplitude than TClower (albeit only slightly for EASM, Figure 4b), which suggests a larger role by TCupper for the seasonal variations in the monsoon indices. This also applies to the EASMIv, TEupper, and TElower, with TEupper playing a bigger role than TElower in forcing the meridional wind shear of the EASM (Figure 4c). The TElower appears to lead the TEupper and EASMIv by about 0.5–1 month. It is unclear what causes this phase difference.

[23] On multiyear (2–7 years) time scales, El Niño-Southern Oscillation (ENSO) is the dominant mode at low latitudes. Figure 5 shows that the 200–500 hPa mean temperature in the spring and summer following a typical El Niño event exhibits warm anomalies up to 0.6°C around 10°S–20°N and cold anomalies around 20°–45°N in both the SASM and EASM sectors, resulting in smaller thermal contrasts and thus weaker SASM (as shown by *Kawamura* [1998]) and EASM in the

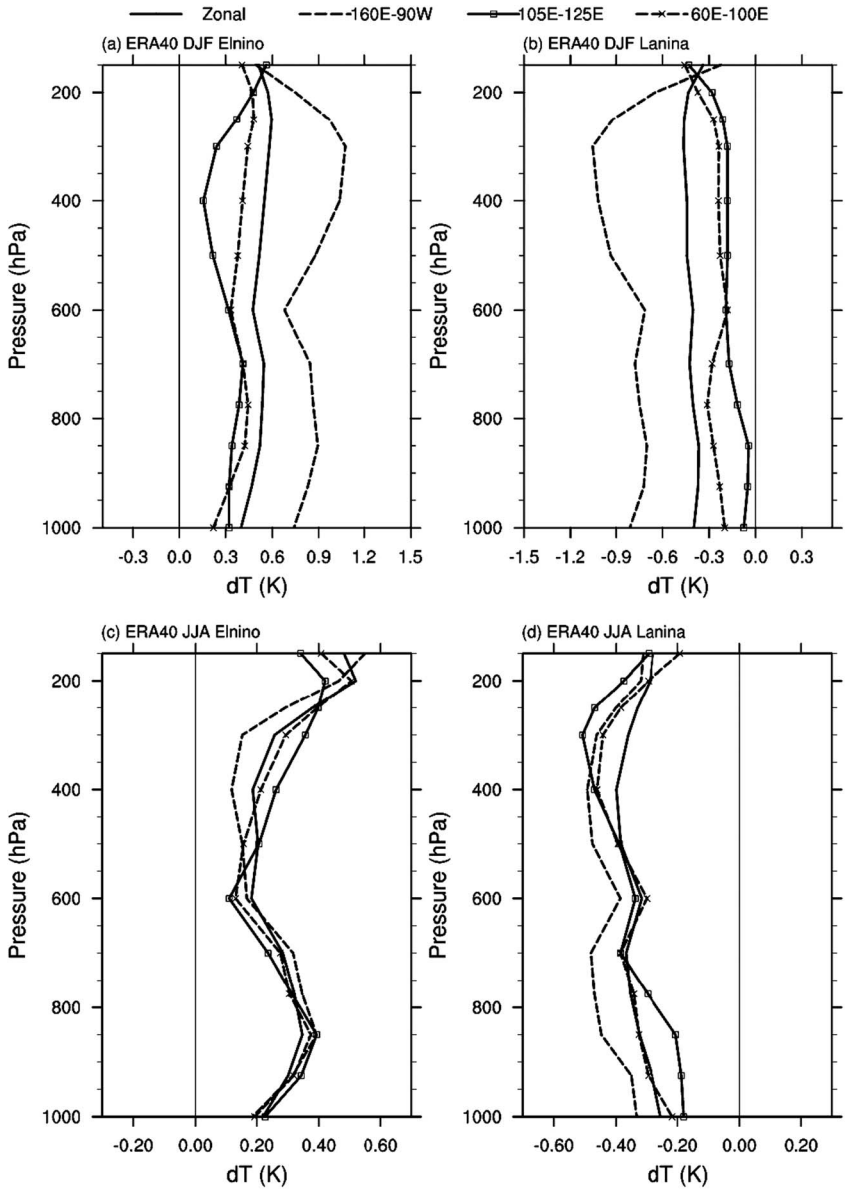

Figure 6. Vertical profiles of composite DJF (top row, ENSO mature phase) and JJA (bottom row, following the ENSO year) temperature anomalies (relative to 1958–2001 mean) during the El Niño (left column) and La Niña years as shown in Figures 5 averaged over 10°S–10°N and four different longitudinal sectors based on ERA-40 reanalysis data. Plots using the NCEP/NCAR reanalysis are similar, except for panel (c) in which the NCEP/NCAR does not show the local maximum around 850 hPa.

summer following an El Niño (Figures 5a–b). The situation is roughly reversed during a typical La Niña event, except that during the summer following a La Niña, 200–500 hPa temperature becomes colder than normal over both the tropics and subtropics, as noticed previously [e.g., *Chou et al*., 2003], leading to small changes to the composite mean thermal contrasts and monsoon indices during the summer (Figures 5d and 5e). We notice that the thermal contrasts also change during the winter and other months (Figure 5) and the SASMI and EASMIu closely follow the TCupper (and TClower) during these months as well, and that TCupper has larger amplitudes than TClower for the ENSO-induced variations. The relationship between EASMIv and TEupper or TElower (Figures 5c and 5f) is weaker than that in the south-north direction. This is expected because ENSO's influence in the northern subtropics is weaker than in the tropics, which directly affects the south-north gradients. The weak relationship for the composite El Niño case (Figure 5c), which includes 1965 and 1972 events, may be also partly due to the spurious cooling over East Asia in the reanalysis data (see Appendix B).

[24] For ENSO-induced variations during ENSO mature phase DJF and the following JJA, both the ERA-40 (Figure 6) and NCEP/NCAR (not shown) reanalysis data show enhanced temperature responses in the mid-upper (500–200 hPa) troposphere compared with near-surface temperature changes over the equatorial region (10°S–10°N) in the central and eastern Pacific Ocean, which is consistent with previous analyses [e.g., *Trenberth and Smith*, 2009]. Over the SASM and EASM sectors, this enhancement is evident only in the JJA following the ENSO year but not in

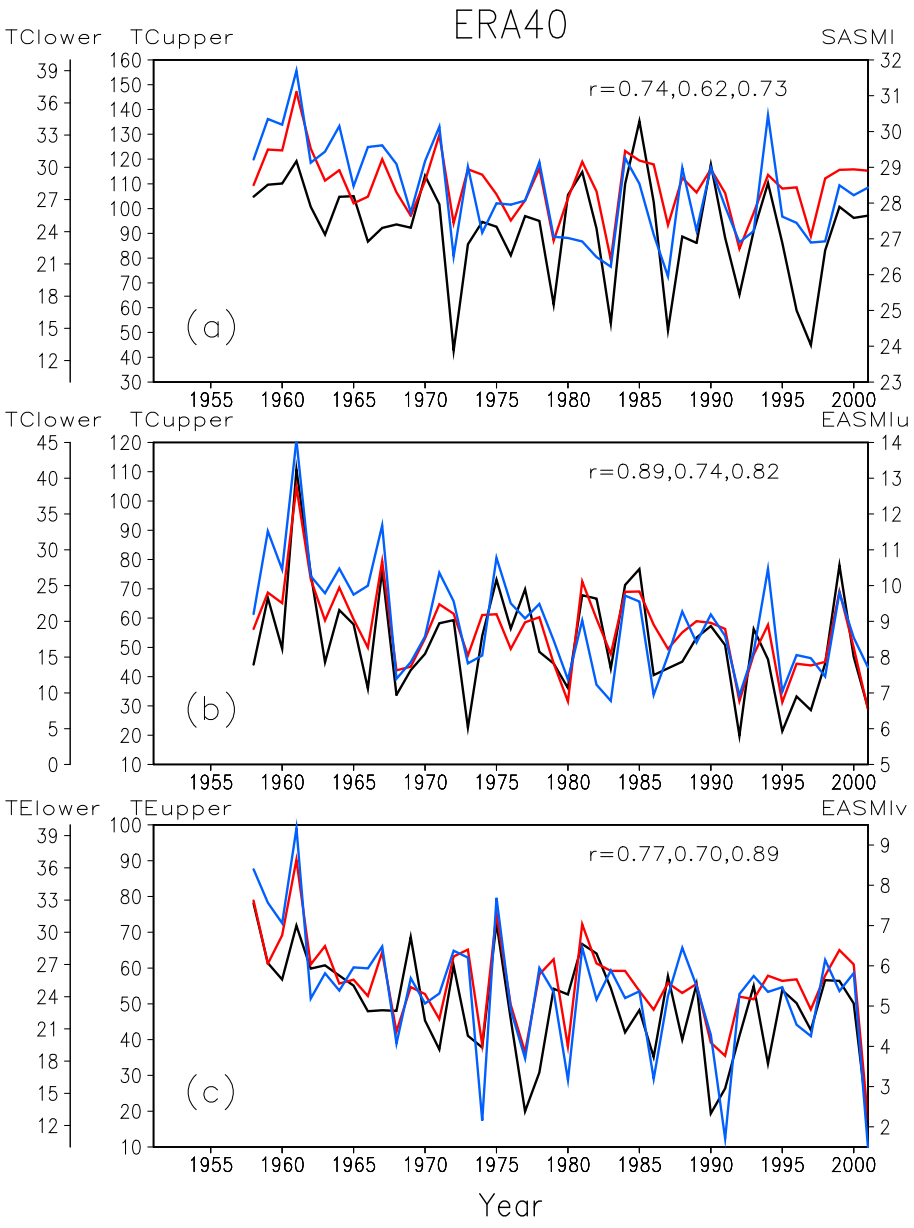

Figure 7. (a) Time series of the JJA SASMI (black), upper (200–500 hPa, TCupper, in gpm, red) and lower (500–700 hPa, TClower, in gpm, blue) tropospheric south-north thermal contrast based on ERA-40 data. (b) same as Figure 7a but for EASMIu (black) and the south-north thermal contrast over the EASM sector (105°–125°E) and TClower of 500–850 hPa. (c) Time series of the JJA EASMIv (black) and the upper (200–500 hPa, TEupper, in gpm, red) and lower (500–850 hPa, TElower, in gpm, blue) tropospheric west-east thermal contrast. The r values are, from left to right, the correlation coefficient between the black and red lines, the black and blue lines, and the red and blue lines. See section 2 for more details.

the ENSO mature phase DJF (Figure 6), due to tropical wave dynamics interacting with convection [*Chiang and Sobel*, 2002; *Su and Neelin*, 2002]. This suggests that ENSO-induced tropical SST variations can affect the Asian summer monsoons more effectively through their influences on the mid-upper tropospheric thermal contrast TCupper than through the mid-lower tropospheric thermal contrast TClower.

[25] Figure 7 shows the time series of JJA SASMI, EASMIu, and EASMIv and their corresponding thermal contrasts from 1958 to 2001 based on the ERA-40 data. First, the scales for TClower (TElower) are about a factor of three smaller than TCupper (TElower) for both SASM and EASM, suggesting that the mean and variations of TClower (TElower) are about one third of those of TCupper (TEupper). Thus, the mid-upper tropospheric thermal gradients are three times more important than the mid-lower tropospheric thermal contrasts in explaining the variations in the monsoon circulation intensity (cf. Figure 3). Second, TCupper (TEupper) and TClower (TElower) are highly correlated on interannual to longer time scales. Finally, the monsoon indices are highly correlated with both the mid-upper and mid-lower tropospheric thermal contrasts, although the correlation with the TCupper (TEupper) is stronger (see the *r* values in Figure 7).

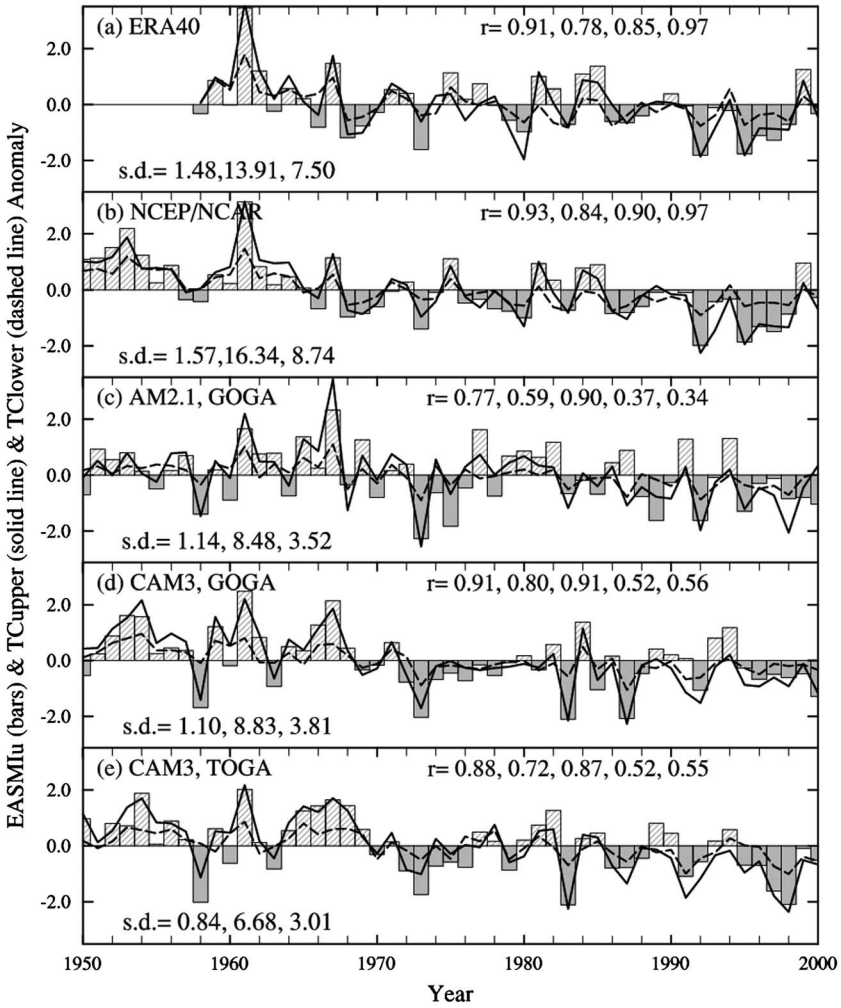

Figure 8. Time series of (normalized) JJA anomalies of the East Asian summer monsoon U index (EASMIu, bars) and the associated north-south thermal contrast in the mid-upper (TCupper, solid line) and mid-lower (TClower, dashed line) troposphere. The panels from top to bottom are for (a) ERA-40 and (b) NCEP/NCAR reanalysis, (c) GFDL AM2.1 GOGA runs, (d) NCAR CAM3 GOGA runs, and (e) NCAR CAM3 TOGA runs. The values are in units of standard deviation (s.d.) and TClower is in units of TCupper's s.d. The values of the s.d. are listed at the lower-left corner of each panel from left to right, respectively, for EASMIu, TCupper and TClower. The correlation coefficient (r) values are for, from left to right, EASMIu vs. TCupper, EASMIu, vs. TClower, TCupper vs. TClower, and for the bars between ERA-40 and NCEP/NCAR reanalysis (top two panels), or for the bars between ERA-40 and the simulated, and NCEP/NCAR and the simulated (lower three panels). See section 2 for definitions for the EASMIu, TCupper, and TClower. Note that the bar charts for a slightly different version of the EASMIu in Figures 8b and 8c were shown previously *Li et al*. [2010].

[26] Figures 7b and 7c also show decreasing trends since the late 1950s in the thermal contrasts in both the south-north and west-east directions and in both the upper and lower troposphere for the EASM. As a result, both the zonal (EASMIu) and meridional (EASMIv) monsoon wind shears have weakened since the late 1950s. These decreasing trends are also evident in the longer NCEP/NCAR reanalysis data (Figures 8b and 9b), and are consistent with other evidence of EASM weakening [*Yu et al*., 2004; *Yu and Zhou*, 2007; *Zhou et al*., 2009a], thus providing increased confidence in these trends. However, much of the decreases occurred around the middle 1960s and these downward trends may be enhanced by a spurious cooling over East Asia in the reanalysis data (see Appendix B). For the SASM (Figure 7a), there are some decreases from 1958 to 1970; thereafter, the SASMI, TCupper, and TClower are quite stable.

[27] The weakening in the south-north thermal contrast over the EASM sector and in EASMIu is broadly captured by both the NCAR (CAM3) and GFDL (AM2.1) AGCMs forced with observed SSTs over the global oceans (referred to as GOGA runs) (Figures 8c and 8d). Furthermore, most of these downward trends are reproduced by the CAM3 forced with observed SSTs only in the tropics (i.e., no year-to-year SST changes in the extratropics, referred to as TOGA runs) (Figure 8c). These results show that the recent warming in the tropical Indian and Pacific Ocean plays a major role in the weakening of the south-north thermal contrasts that lead to the weakening of the EASMIu reported

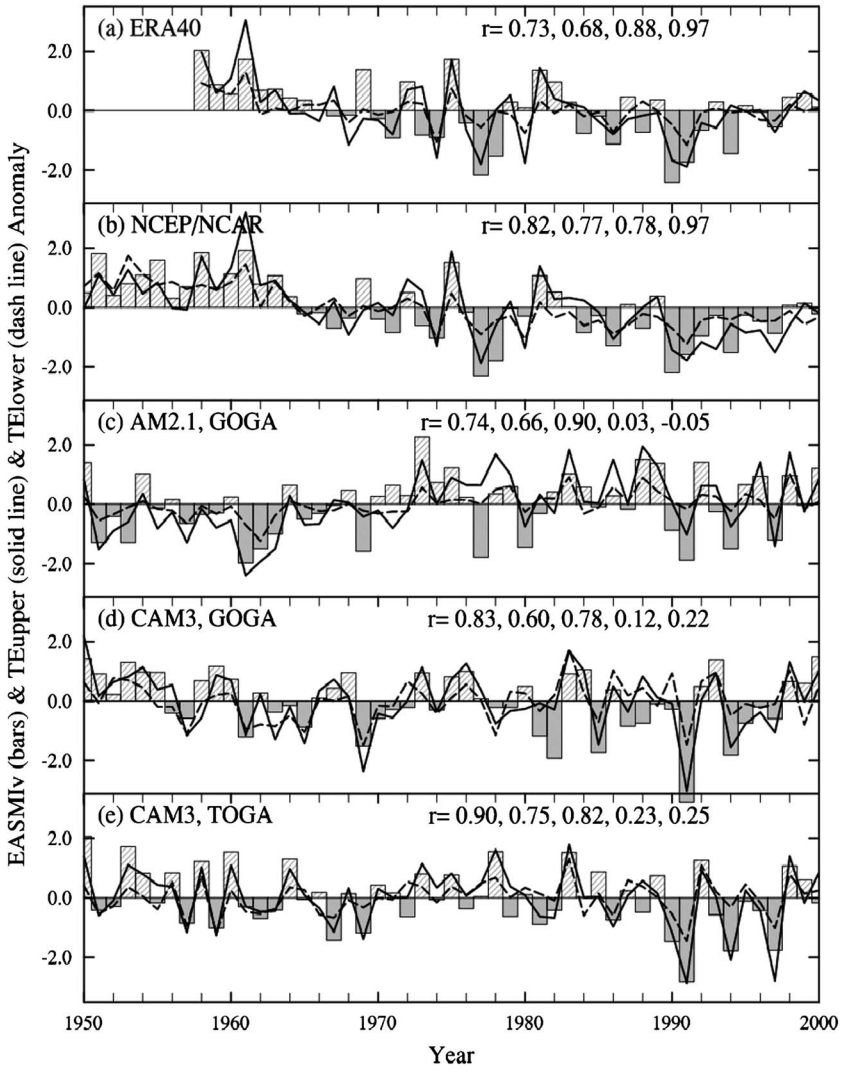

Figure 9. Same as Figure 8 but for the East Asian summer monsoon V index (EASMIv, bars) and the associated thermal contrasts TEupper and TElower over 20°–40°N.

previously [*Li et al*., 2010; *Yang et al*., 2008; *Ding et al*., 2009]. However, some studies [e.g., *Ding et al*., 2009; *Zhao et al*., 2010] also suggest an important role of reduced sensible heating over the TP in the weakening of the EASM in the past 50 years (see Appendix B for more on this). Besides the downward trends, many of the year-to-year variations in the reanalysis TCupper, TClower, and EASMIu are also captured by the models, especially in the CAM3 runs, in which the reanalysis and simulated EASMIu have a correlation of 0.52 or higher (Figures 8d and 8e).

[28] There are, however, substantial differences between the reanalysis and simulated time series shown in Figure 8. For example, the magnitudes of the trends and variations for the three curves are much larger in both the ERA-40 and NCEP/NCAR reanalyses than in the model runs, as reflected by the differences in the standard deviation (s.d., Figure 8). For instance, the s.d. of the EASMIu in the two GOGA runs (TOGA run) is only about 73% (56%) of those in the reanalyses. Furthermore, the s.d. of the TClower is about 53% of the s.d. for TCupper in the reanalyses, compared with the 42–45% in the model runs. The timing of the largest decreases also differs noticeably: from the early to late 1960s in the two reanalyses vs. from the late 1960s to the early 1970s in the models.

[29] The downward trends and year-to-year variations in TEupper, TElower, and EASMIv (Figure 9) in the reanalysis data are not captured as well as those in Figure 8. In fact, the AM2.1 model shows upward trends in these time series (Figure 9c). The CAM3 shows very small trends in both the GOGA and TOGA runs (Figures 9d and 9e). The models' low skill in simulating the zonal thermal contrasts and EASMIv has been noticed previously and attributed to failure to capture the zonal land-sea temperature gradient [*Zhou et al*., 2009c; *Zhou and Zou*, 2010]. This failure partly results from the inherent limitations of SST-forced model runs over the North Pacific and other regions where two-way air-sea interactions are important. The discrepancies between the reanalyses and the model runs shown in Figure 9 are also likely enhanced by the spurious cooling before the early 1970s in the reanalysis data (see Appendix B). Despite the apparent discrepancies, however, both Figures 8 and 9 show strong correlations between the monsoon indices for the EASM and the corresponding thermal contrasts in both the upper and lower troposphere in all the simulations, and

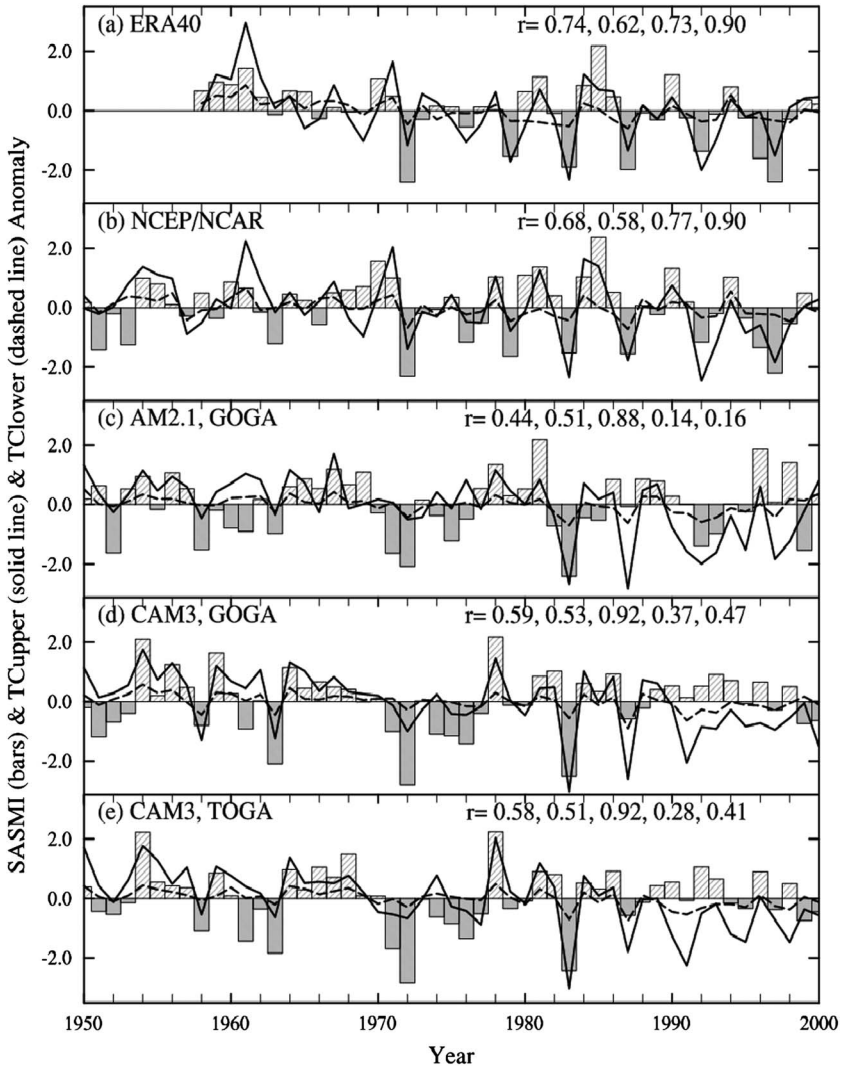

Figure 10. Same as Figure 8 but for the South Asian summer monsoon index (SASMI) and the associated thermal contrasts TCupper (solid line) and TClower (dashed line, in units of TCupper's s.d.) for the sector 60°–100°E.

the correlations are comparable to those in the reanalysis data. Furthermore, the TCupper (TEupper) shows larger variations and changes than TClower (TElower) in both the reanalyses and model simulations. Thus, the wind-shear-based monsoon indices for the EASM are highly correlated with the thermal contrasts in both the upper and lower troposphere, with the mid-upper tropospheric thermal contrast being larger and contributing more than the thermal contrast in the mid-lower troposphere during 1950–2000 in both the reanalyses and model runs.

[30] For the SASM, both the ERA-40 and NCEP/NCAR reanalyses show only slight weakening since the 1950s in the TCupper, TClower, and SASMI (Figure 10). The model simulations also do not show significant trends in these variables. Nevertheless, the model-simulated TCupper variations are larger than TClower, and both are correlated with the simulated SASMI, as in the two reanalyses. However, the correlation between the reanalysis and simulated SASMI is weak and statistically significant only for the CAM3 GOGA case. This weak correlation with reanalysis SASMI is also evident in other SST-forced model simulations and is attributed to a weakening ENSO-monsoon connection (a major basis for the correlation between simulated and reanalysis SASMI) in recent decades [*Zhou et al*., 2009c].

[31] Figure 11 shows the latitude-height cross section of the decadal difference of JJA temperature and wind averaged over the EASM sector from the NCEP/NCAR reanalysis and the model runs. It shows that the models broadly reproduce the reanalysis patterns of the decadal temperature and wind changes in both the GOGA and TOGA runs, with warming at low latitudes and cooling at northern higher latitudes. However, the models show only a small cooling (0.2–0.4°C) from about 40°–50°N, in contrast to a large cooling (up to 2°C) north of about 35°N in the NCEP/NCAR reanalysis (Figure 11). Thus, a large portion of the reduction in the north-south temperature gradient throughout the troposphere over East Asia (left panels in Figure 11a) and thus in TCupper and TClower for EASM (Figure 8) in the reanalysis result from the cooling north of about 35°N, while the weakening in north-south thermal contrasts in the models mainly comes from the warming in the tropical troposphere. In

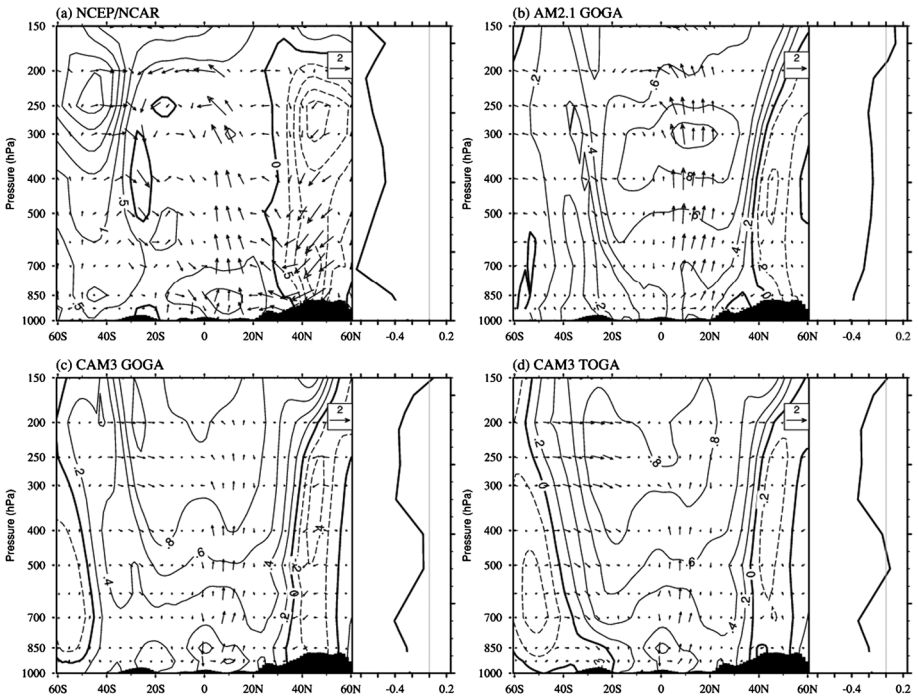

Figure 11. Latitude-height cross section of the decadal difference (1977–2000 minus 1951–1976) for 105°–125°E averaged JJA temperature (contours, K, the interval is 0.5 K for Figure 11a and 0.2 K for Figures 11b–11d) and winds (arrows) from (a) NCEP/NCAR reanalysis, (b) GFDL AM2.1 GOGA runs, (c) NCAR CAM3 GOGA runs, and (d) NCAR CAM3 TOGA runs. The vertical profile of the north (20°–40°N) minus south (10°S–10°N) difference (K) of the decadal temperature change is shown in the right panel. ERA-40 data show changes similar to Figure 11a. Decadal changes are small for the South Asian summer monsoon sector (60°–100°E) and thus not shown.

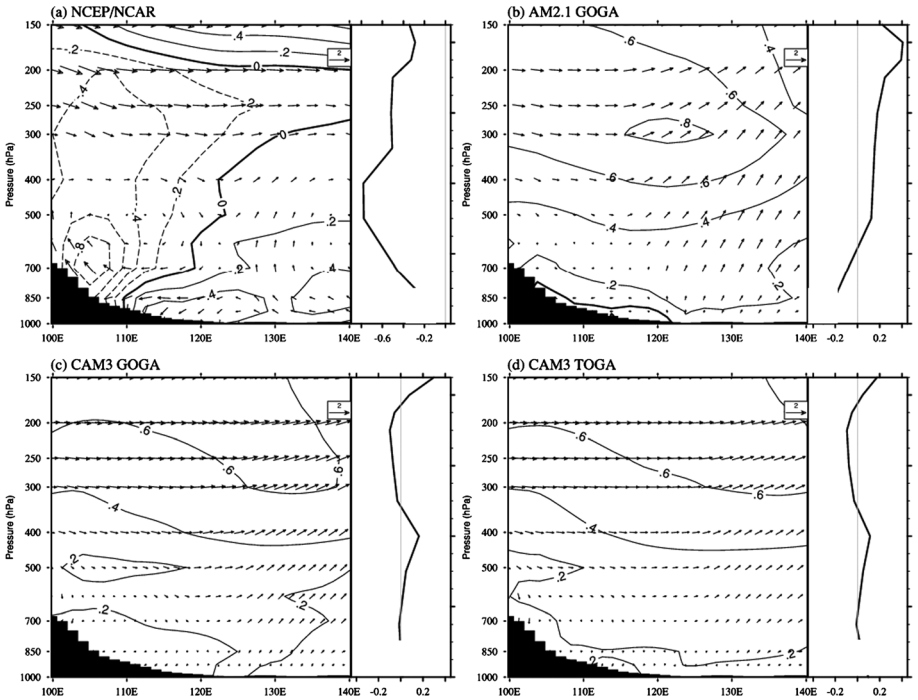

Figure 12. Longitude-height cross section of the decadal difference (1977–2000 minus 1951–1976) for 20°–40°N averaged JJA temperature (contours, K) and winds (arrows) from (a) NCEP/NCAR reanlaysis, (b) GFDL AM2.1 GOGA runs, (c) NCAR CAM3 GOGA runs, and (d) NCAR CAM3 TOGA runs. The vertical profile of the west (105°–120°E) minus east (135°–150°E) difference (K) of the decadal temperature change is shown in the right panel. ERA-40 data show changes similar to Figure 12a.

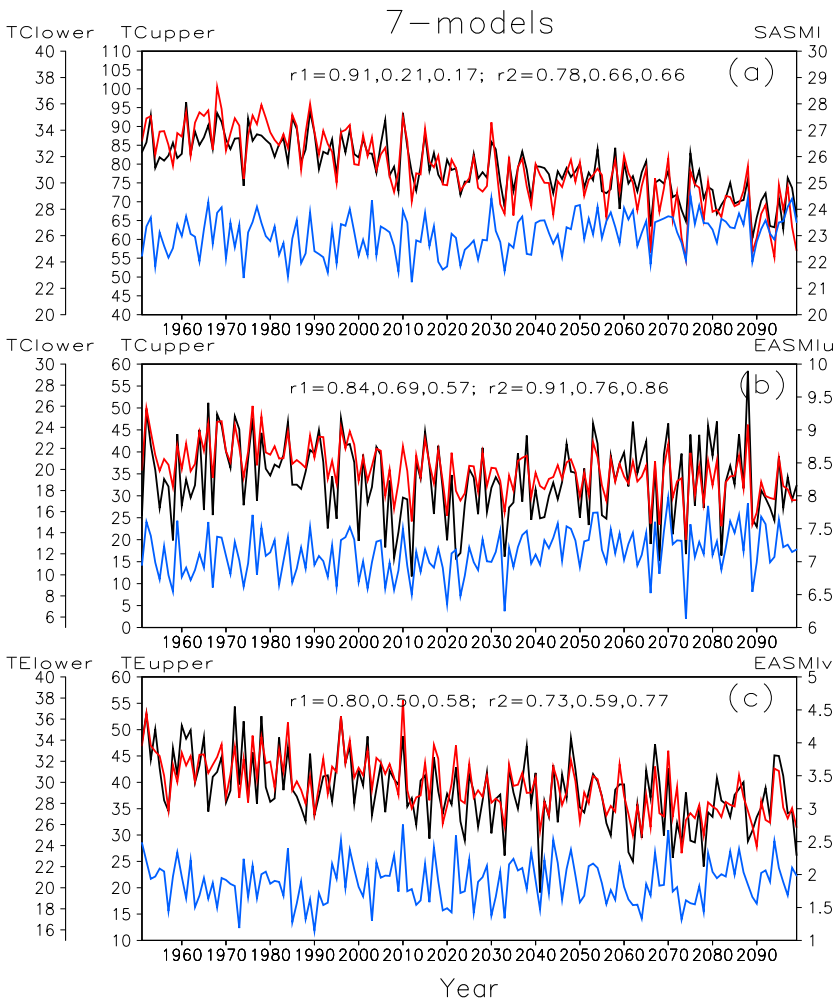

Figure 13. Seven-model ensemble-mean time series of JJA (a) SASMI (black) and the associated mid-upper (200–500 hPa, TCupper, in gpm, red) and mid-lower (500–700 hPa, TClower, in gpm, blue) tropospheric south-north thermal contrasts. (b) Same as Figure 13a but for EASMIu and its associated TCupper and TClower (for 500–850 hPa). (c) Same as Figure 13a but for EASMIv and its associated upper (TEupper, red) and lower (TElower, blue) tropospheric west-east thermal contrasts. Also shown are the correlation coefficients between the lines with (r1) and without (r2) the long-term trends; they are, from left to right, for black vs. red, black vs. blue, and red vs. blue lines. See section 2 for details of the definition for these terms. The A1B scenario was used.

Appendix B, we show that the cooling over East Asia in the reanalysis may be spurious. The model runs also show enhanced warming in the tropical mid-upper troposphere (500–200 hPa), in contrast to both the NCEP/NCAR (Figure 11a) and ERA-40 (not shown) reanalysis data, whose lack of the enhanced upper tropospheric response might be related to problems in radiosonde data [*Santer et al*., 2005].

[32] Consistent with Figure 9, Figure 12 shows that the model runs fail to capture the land-ocean thermal contrast in the west-east direction for EASM seen in the reanalysis. In fact, the GFDL AM2.1 produces increased land-ocean temperature differences above ~600 hPa in its GOGA runs (Figure 12b), resulting in an upward trend in TEupper and EASMIv (Figure 9c). As mentioned above, this discrepancy may be due to models' inability to capture the zonal land-sea temperature contrasts in SST-forced experiments and errors in the reanalysis data.

4.2. Relationship Under a Global Warming Scenario

[33] Using thermal contracts based on temperature differences for TClower (in contrast to the thickness-based TClower used here) and thickness difference for TCupper, *Sun et al*. [2010] examined the relationship between SASMI and the thermal contrasts in the lower and mid-upper troposphere under a global warming scenario. They found that the long-term trend in SASMI in the 21st century follows only with the thermal contrast change in the mid-upper troposphere and is the opposite to the thermal contrast trend in the lower troposphere. Using their definitions of the thermal contrasts and an EASMI as the mean meridional wind at 850 hPa (V_{850}) over East Asia, *Sun and Ding* [2011] extended the analysis to include the EASM. They found that the changes in the V_{850}-based EASMI are consistent with the changes in the lower-tropospheric thermal contrast in the 21st century. Here we examine the relationship using our definitions for

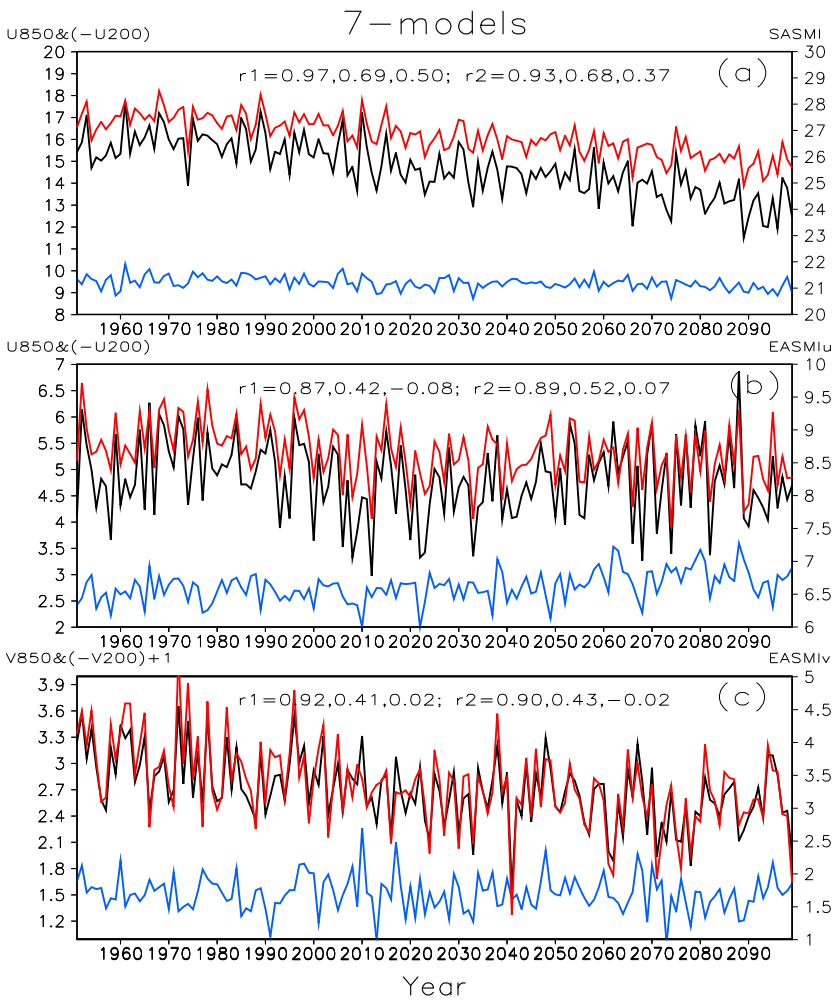

Figure 14. Same as Figure 13 but for the time series of monsoon indices (black) and their corresponding wind components at 850 hPa (blue) and 200 hPa (red) levels. Note the 200 hPa winds are multiplied by −1, and shifted by +1 for (−V200) in order to be separated from the other lines. Also shown are the correlation coefficients between the lines with (r1) and without (r2) the long-term trends; they are, from left to right, for black vs. red, black vs. blue, and red vs. blue lines. See section 3 for details of the definition for these terms. The A1B scenario was used.

the thermal contrasts and monsoon indices, which are very different for EASM (see section 2) from the V_{850}-based EASMI used by *Sun and Ding* [2011]. We perform this analysis also from a different perspective, namely, to quantify the relative roles of TCupper and TClower under a global warming scenario, which is hard to do using the TCupper and TClower of *Sun et al.* [2010] since they have different units.

[34] Figure 13a shows that the model-simulated SASMI weakens in the 21st century, together with a decreasing mid-upper tropospheric thermal contrast TCupper, but the thermal contrast in the mid-lower troposphere (TClower) strengthens. This result confirms the findings of *Sun et al.* [2010], and the weakening SASMI is consistent with *Kripalani et al.* [2007a]. Without the opposite trends, TClower still is significantly correlated with TCupper (r = 0.66) and with SASMI (r = 0.66), but with smaller variations than those of TCupper (Figure 13a, note the different scales). This suggests that different physical processes are behind the long-term trend and year-to-year variations in TClower.

[35] For the EASM, EASMIu and TCupper are highly correlated (r = 0.84), and both show small downward trends mostly from the 1990s to the 2030s, while TClower shows a slight increase in the late half of the 21st century (Figure 13b). As a result, EASMIu correlates significantly with both TCupper and TClower, although TClower has much smaller mean and variations than TCupper. For EASMIv, a steady downward trend from 1950 to 2099 is accompanied by a similar downward trend in TEupper, while TElower shows no trend (Figure 13c). EASMIv correlates strongly with TEupper and, to a lesser extent, with TElower also, although the downward trend in EASMIv weakens the correlation slightly.

[36] The decrease in SASMI results mainly from a downward trend in the mean −U200 averaged over 0°–20°N and 60°–100°E, while the mean U850 only shows small changes (Figure 14a). These wind trends are consistent (through equation (A1) in Appendix A) with the temperature changes over the SASM sector (Figure 15a), which show a maximum warming in the tropical upper troposphere and similar warming from the tropics to midlatitudes below about

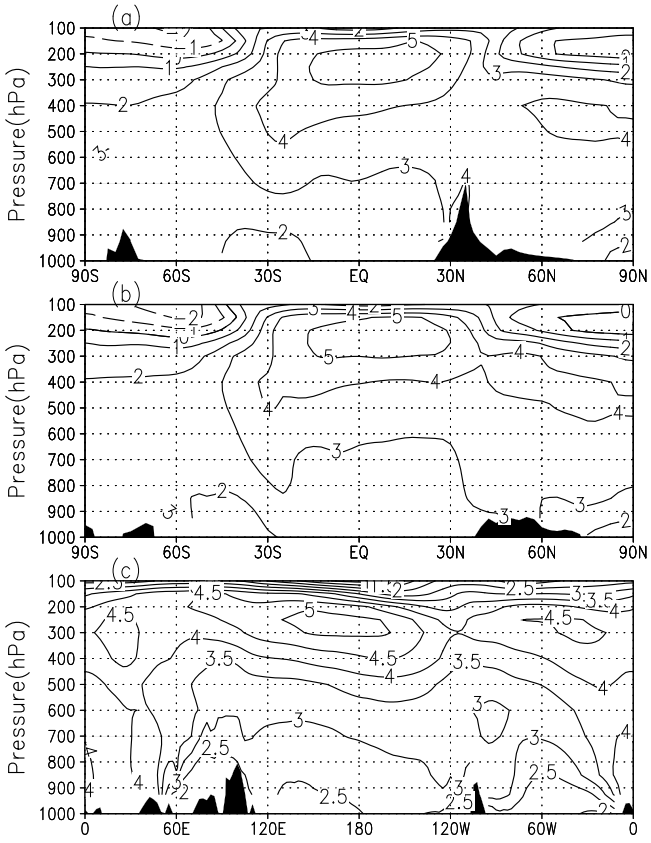

Figure 15. (a) Seven-model ensemble mean latitude-height cross-section of JJA temperature change (°C) from 1980–1999 to 2080–2099 under SRES A1B emissions scenario and the mean topography (dark shading) averaged between 60° E and 100°E. (b) Same as Figure 15a but for the EASM sector (105°–125°E). (c) Same as Figure 15a but for longitude-height cross section of the temperature changes averaged over 20°–40°N.

500 hPa. For the EASM sector, the upper tropospheric maximum warming extends farther into the northern subtropics (Figure 15b), thus reducing the changes in the meridional temperature gradient in the upper troposphere. In the lower troposphere, the warming over the East Asian continent is slightly higher than over the tropics on the same pressure level (Figure 15b). These warming patterns result in slight decreases in the mean −U200 and small increases in the mean U850 averaged over 10°–30°N and 105°–125°E (Figure 14b), again through equation (A1).

[37] The maximum warming in the tropical upper troposphere is a common feature in all climate models that result from enhanced latent heating from deep convection [*Dai et al*., 2001; *Santer et al*., 2005]. This warming maximum also appears in the upper troposphere over the North Pacific Ocean in the 20°–40°N zone (Figure 15c), which reduces the west-east thermal contrast TEupper and thus weakens the mean −V200 in Figure 14c. In the lower troposphere, the zonal gradient of the temperature changes is small (Figure 15c), resulting in small changes in the mean V850 (Figure 14c).

[38] Thus, the weakening of the monsoon indices SASMI and EASMIv are mainly due to weakening upper-level winds at 200 hPa, while the low-level winds at 850 hPa change little. This is consistent with the studies by *Sun and Ding* [2010, 2011], who show a weak increasing trend in an EASM index based on 850 hPa meridional winds. The weakening in upper-level winds results from reduced land-ocean thermal contrasts due to a warming maximum in the upper troposphere over the tropical oceans and the North Pacific Ocean as a result of enhanced convective latent heating. These circulation changes are consistent with model-simulated increases in summer monsoon precipitation over South and East Asia [*Kitoh*, 2006; *Kripalani et al*., 2007a, 2007b; *Sun and Ding*, 2010; *Bhaskaran*, 2012], which result primarily from higher specific humidity in the lower troposphere over the regions, similar to the rich-get-richer mechanism under global warming for the tropics [*Chou et al*., 2009]. However, we noticed that current models have difficulties in simulating historical changes in EASMIv and the zonal thermal gradients (Figures 9 and 12), and the changes in the EASM winds under a warming scenario can be model dependent. This suggests that the model-predicted future changes for EASMIv and the zonal thermal gradients need to be interpreted cautiously.

5. Causes of the Land-Sea Thermal Contrasts in the Free Troposphere

[39] There are many causes for the changes in the tropospheric land-sea thermal contrasts on different time scales. Here we discuss some of these causes. For the annual cycle (Figure 4), the large seasonal variations of mid-upper tropospheric temperatures over the Asian continent and thus the seasonal variations in TCupper and TClower are caused mainly by solar heating (largely through the sensible heating released by the TP) and further enhanced by latent heating from monsoon rainfall for TCupper, as the seasonal variations over the tropical oceans are comparatively small (Figure 4). This also applies to TEupper and TElower for the EASM in the west-east direction, as the seasonal variations of tropospheric temperatures are larger over the East Asian continent than the North Pacific Ocean (Figure 4). For ENSO-induced multiyear variations (Figure 5), it is evident that the mid-upper tropospheric temperature responses to ENSO SST anomalies over both the tropical Indian Ocean and the Asian continent are responsible for the TCupper (and possibly TClower) variations associated with ENSO. This is consistent with the findings of *Zhang and Zhou* [2012], who showed that the two leading modes of the upper tropospheric temperature multiyear variability over East Asia result from remote tropospheric response to ENSO SST anomalies and local moist processes.

[40] On decadal and longer time scales, changes in tropospheric temperatures over both the tropical oceans and the extratropical Asian land can contribute to the changes in the TCupper and TClower, although we have emphasized that the tropical oceans can effectively influence Asian monsoons through their impacts on TCupper. For example, both the warming in tropical troposphere associated with higher SSTs in the Indian Ocean and the extratropical cooling over the Asian continent (Figure 11) have contributed to the weakening in TCupper and TClower over the EASM sector (Figure 8), although some of the tropospheric cooling over Asia may be spurious. For the global warming scenario in the 21st century, the changes in the tropospheric land-sea thermal contrasts depend critically on the temperature change patterns in the troposphere (Figure 15). For the SASM sector, the latent heating-enhanced

warming is concentrated in the upper tropical troposphere (Figure 15a), leading to a decline in TCupper for SASM. In the EASM sector, the enhanced upper tropospheric warming spreads over to the Asian continent (Figure 15b), leading to small changes in TCupper (Figure 13b). In the west-east direction, the enhanced warming in the upper troposphere over the North Pacific Ocean (Figure 15c) due to enhanced latent heating again leads to a decline in TEupper (Figure 13c). In all these cases, the tropical and extratropical warming in the mid-lower troposphere are comparable, leading to small changes in TClower and TElower.

[41] Thus, the model-predicted TCupper and TEupper changes and thus SASM and EASM responses to future GHG forcing depend critically on the enhanced warming in the upper troposphere. Although it is generally accepted that enhanced latent heating from more vigorous convection under warmer climates is the main cause for the enhanced warming in the upper troposphere at low latitudes [*Dai et al*., 2001; *Santer et al*., 2005], more investigation is needed on the exact processes leading to the enhanced warming giving its importance to Asian land-sea thermal contrasts and monsoon circulations. Similarly, further analyses are needed to quantify the contribution to TCupper and TEupper from the latent heating released during monsoon rainfall over the Asian continent, e.g., by examining the relationship between monsoon rainfall and TCupper or TEupper. The latter will also help us understand the relationship between the monsoon circulation indices (SASMu, EASMu, EASMv) and monsoon rainfall. These issues need to be addressed in future studies.

6. Summary and Concluding Remarks

[42] Previous analyses [e.g., *Webster*, 1987] and the mean thermal structure and wind fields over the Asian sector show a larger mean land-ocean thermal gradient in the mid-upper (200–500 hPa, TCupper) than in the lower (500–850 hPa, TClower) troposphere during summer. Since a TCupper with a larger mean does not necessarily play a bigger role in explaining variations and changes in the SASM and EASM circulations, we have compared the variations in TCupper and TClower and their relationship with the corresponding Asian monsoon indices on seasonal to decadal time scales to further quantify their relative roles in driving the SASM and EASM circulations. Using the TCupper and TClower, we also examined the historical changes in the intensity of the EASM and SASM, and analyzed model-projected future changes for them. We adopted *Webster and Yang*'s [1992] approach and defined the monsoon indices for the SASM and EASM using the regionally averaged wind shear between 850 hPa and 200 hPa levels as a measure of the monsoon circulation intensity. The gradient in layer geopotential height thickness (ΔZ) was used to define the land-ocean thermal contrasts in the atmosphere.

[43] It is found that the mean and variations of TCupper (TEupper) over the SASM and EASM sectors are about three times larger and thus three times more important than TClower (TElower) in driving the mean SASM and EASM circulations and explaining their variations. This is partly due to larger land-ocean temperature gradients in the mid-upper troposphere than in the mid-lower troposphere resulting from convective latent heating over land. As expected from the thermal wind relation, the regionally averaged monsoon indices SASMI, EASMIu, and EASMIv are highly correlated with their respective TCupper and TClower, or TEupper and TElower for EASMIv (as defined in section 2), from seasonal to multidecadal time scales. Although the thermal contrasts in the upper and lower troposphere are usually correlated with each other, the monsoon indices have a stronger correlation with the land-ocean thermal contrast in the mid-upper troposphere than in the mid-lower troposphere because of their different roles in determining the strength of the Asian summer monsoon circulations.

[44] Both the ERA-40 and NCEP/NCAR reanalysis data show a weakening trend in the U (EASMIu) and V (EASMIv) indices for the EASM since the 1950s, especially around the middle 1960s, and this apparent weakening is caused by a reduction in both TCupper and TClower for EASMIu and TEupper and TElower for EASMIv. A portion of the EASM weakening seen in the two reanalyses is likely real resulting from the warming in the tropical troposphere. Further examination shows that some of the weakening may result from a large spurious cooling over East Asia that occurred primarily from the 1950s to the early 1970s and is centered northeast of the TP with a maximum around 300 hPa.

[45] Forced with observed SST changes since 1950, especially in the tropics, both the NCAR CAM3 and GFDL AM2.1 models were able to capture the downward trends and many of the year-to-year variations in EASMIu, TCupper, and TClower seen in the reanalysis data, and reproduced the warming in the tropical troposphere. However, the models show only a small cooling (0.2–0.4°C) from about 40°–50°N, in contrast to a large cooling (up to 2°C) north of about 35°N in the NCEP/NCAR reanalysis. The models also do not show the downward trends in EASMIv, TEupper, and TElower over the East Asia to North Pacific region seen in the reanalyses, which are strongly influenced by the spurious cooling over East Asia. For the SASM, its circulation index SASMI and the associated thermal contrasts TCupper and TClower only show very weak downward trends in both the two reanalyses and SST-forced model simulations.

[46] Under the A1B scenario in the 21st century, results from seven selected models that simulate the present-day SASM relatively well show a robust weakening in the SASM circulation resulting primarily from a weakening in upper-level winds (−U200). This weakening in (−U200) is caused by a reduction in TCupper resulting from enhanced warming in the tropical upper troposphere due to increased convective latent heating. These results confirm the findings of *Sun et al*. [2010]. Over the EASM sector, the enhanced warming in the tropical upper troposphere extends farther to the northern subtropics, resulting in small decreases in TCupper, −U200, and EASMIu; whereas the mid-lower tropospheric thermal contrast and low-level zonal wind U850 increase slightly. Along the 20°–40°N latitude zone, the models predict a maximum warming in the upper troposphere over the North Pacific Ocean. This results in a reduction in the summer East Asia to North Pacific thermal contrast in the mid-upper troposphere (TEupper), which leads to a weakening in upper-level winds (−V200) and the V index EASMIv for the EASM. For both the SAMS and EASM, changes in low-level monsoon winds

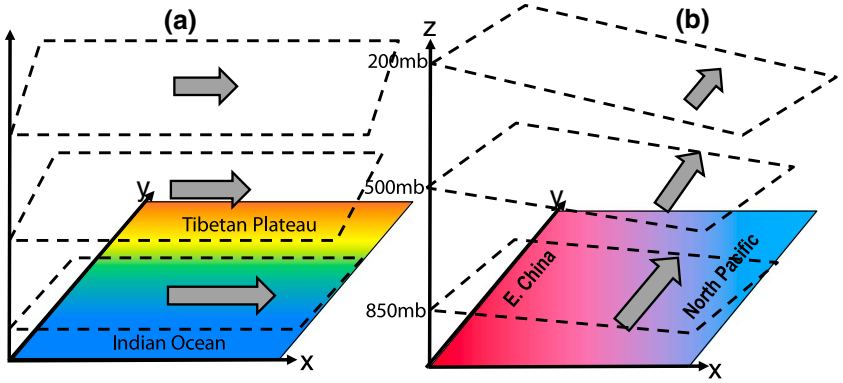

Figure A1. Schematic diagram for temperature gradient-induced thermal winds in (a) zonal and (b) meridional direction.

are relatively small. Combined with increased specific humidity under higher temperatures, this would suggest increased summer monsoon rainfall over South and East Asia, consistent with previous analyses of monsoon rainfall changes over Asia [*Kripalani et al*., 2007a, 2007b; *Sun and Ding*, 2010; *Bhaskaran*, 2012].

[47] Our results demonstrate that the thermal contrast in the mid-upper troposphere plays a more dominate role than the contrast in the mid-lower troposphere in determining the strength and variations of the Asian summer monsoon circulations, and that there are cases where the thermal contrasts in the upper and lower troposphere may be decoupled, such as in the 21st century global warming case where TCupper and TClower for the SASM and TEupper and TElower for the EASM show opposite trends.

[48] The above results also show that variations and changes in tropical SSTs, such as those associated with ENSO and global warming, can affect extratropical monsoons more effectively through their influences on the land-ocean thermal contrast in the upper troposphere than in the lower troposphere. This is expected given the enhanced temperature response to tropical SST anomalies in the tropical upper troposphere due to convective latent heating and the rapid zonal advection in tropical free troposphere. Thus, the mid-upper tropospheric thermal contrast provides an effective mechanism through which tropical SSTs can influence extratropical monsoons over Asia and possibly other regions. Our findings also stress the need to use the tropospheric, especially mid-upper tropospheric, thermal contrast, rather than the near-surface temperature gradients, in studying monsoons and in interpreting model-simulated monsoon changes.

Appendix A: Monsoon and Thermal Winds

[49] We review the following thermal wind equations on a pressure surface [*Holton*, 2004] for understanding the role of thermal contrasts in determining the intensity of a monsoon circulation:

$$U(p_1) - U(p_o) = -\frac{R}{f}\left(\frac{\partial \overline{T}}{\partial y}\right)\ln\left(\frac{p_o}{p_1}\right) = -\frac{1}{f}\frac{\partial(\Phi_1 - \Phi_0)}{\partial y} \quad \text{(A1)}$$

$$V(p_1) - V(p_o) = \frac{R}{f}\left(\frac{\partial \overline{T}}{\partial x}\right)\ln\left(\frac{p_o}{p_1}\right) = \frac{1}{f}\frac{\partial(\Phi_1 - \Phi_0)}{\partial x} \quad \text{(A2)}$$

where p_1 and p_o denote two pressure levels; U and V are, respectively, zonal (x-direction) and meridional (y-direction) wind components; $\overline{T} = \int_{p_1}^{p_0} T\, d\ln p / \ln\left(p_0/p_1\right)$ is the (log-pressure weighted) *mean temperature* between levels p_o and p_1; Φ_1 and Φ_o are the geopotential at levels p_1 and p_o, respectively; R is the gas constant of air; and f is the Coriolis parameter. Note that here we use geopotential height Z, which equals to Φ/g_o, where $g_o = 9.80665\ \mathrm{m\,s^{-2}}$ [*Holton*, 2004]. These equations and the schematic diagrams of Figure A1 show that it is the horizontal gradient of the mean temperature $(\overline{T})$ within the whole layer from p_o to p_1 that determines the vertical wind shear between the levels p_o and p_1, and that the zonal wind shear is determined by the meridional (south-north) temperature gradient while the meridional wind shear is determine by the zonal (west-east) temperature gradient. For the SASM, the south-north temperature gradient $(\partial\overline{T}/\partial y)$ between the tropical Indian Ocean (TIO) and the TP is the driving force for its mostly zonal winds (Figure 1). For the EASM, it is more complicated as it is influenced by both the south-north and west-east temperature gradients (Figure A1, Figure 1).

[50] For monsoon intensity, low-level (e.g., 850 hPa) winds are most relevant as they are close to people living on Earth. Based on equations (A1) and (A2), one might think that only low-level thermal gradients are important for low-level monsoon winds. This is not entirely true because the upper- and lower-level winds are coupled to form a complete monsoon circulation [*Holton*, 2004]. That is, the low-level convergent winds are dynamically coupled with the upper-level divergent winds in a monsoon circulation. Suppose there is no horizontal temperature gradient in the lower-troposphere (up to 700 hPa) and thus the zonal wind at 700 hPa (U_{700}) is the same as that at 850 hPa (U_{850}). If the layer between 700 hPa and 200 hPa contains a large south-north temperature gradient, then, according to equation (A1), U_{700} should equal to the zonal wind at 200 hPa (U_{200}) plus the thermal wind in the upper layer, i.e., $U_{850} = U_{700} = U_{200} + \frac{1}{f}\frac{\partial(\Phi_{700} - \Phi_{200})}{\partial y}$. In other words, thermal contrasts within the whole troposphere can affect the low-level monsoon winds because of their vertical coupling. Also note that the thermal contrast only affects the vertical wind shear; other factors (e.g., large-scale synoptic systems) can also affect the winds at a given level.

[51] For the SASM, most of the TP is above 850 hPa. Thus, it does not make sense to compare the near-surface or lower-

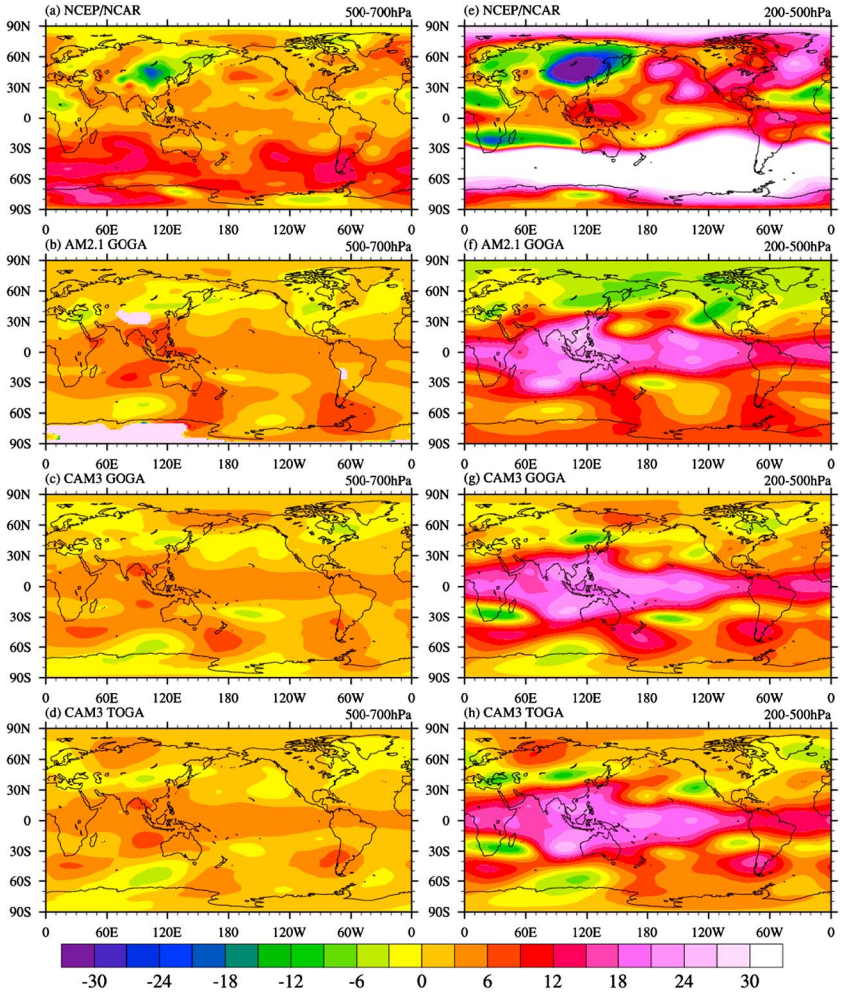

Figure B1. The decadal changes (1977–2000 minus 1950–1976) in the JJA layer thickness (in gpm) for (left) 500–700 hPa and (right) 200–500 hPa layers from (a, e) NCEP/NCAR reanalysis, (b, f) GFDL AM2.1 GOGA runs, (c, g) NCAR CAM3 GOGA runs, and (d, h) NCAR CAM3 TOGA runs.

tropospheric (below about 700 hPa) temperatures or Z over the TP and TIO, since they are either not on the same pressure level, or does not exist for the TP.

Appendix B: The Apparent Tropospheric Cooling Over East Asia

[52] To further examine the tropospheric thermal response to observed SST forcing, Figure B1 compares the decadal changes (1977–2000 minus 1950–1976) in the JJA thickness of the 500–700 hPa and 200–500 hPa layers from AM2.1 and CAM3 runs and the NCEP/NCAR reanalysis. The ERA-40 (not shown) exhibits patterns broadly comparable to the NCEP/NCAR reanalysis, although the magnitude of the cooling over East Asia is reduced in the ERA-40. In both the models, the tropical troposphere, especially for 200–500 hPa, has the largest thickening or warming in response to recent SST increases. Although the NCEP/NCAR reanalysis also shows a large warming response in the tropical troposphere, especially for 200–500 hPa, the largest warming appears to be over the Southern Oceans in the NCEP/NCAR (and ERA-40) reanalysis. Another unusual feature is the large cooling over East Asia centered around (43°N, 106°E) in the NCEP/NCAR (Figure B1e) reanalysis and around (40°N, 102°E) in the ERA-40 (not shown). This tropospheric cooling is very weak in the AM2.1 and CAM3 runs (Figure B1b–B1h). The large cooling over East Asia in both the NCEP/NCAR and ERA-40 reanalyses contributes significantly to the downward trends in the land-ocean thermal contrasts and EASMIu and EASMIv for the EASM in the reanalyses, especially in the west-east direction (cf. Figures 8 and 9), but not so much in the model runs in which the thermal responses over the oceans play a more important role. This helps partly explain why the models failed to simulate the TEupper, TElower, and EASMIv from the reanalyses (cf. Figure 9), although inherent limitations of the SST-forced runs is also part of the reason.

[53] Many studies [e.g., *Yu et al*., 2004; *Yu and Zhou*, 2007; *Zhou and Zhang*, 2009] have investigated the large cooling over East Asia in the reanalysis data, which peaks around 300 hPa and in April and July–August [*Yu and Zhou*, 2007] and occurred primarily from the 1950s to the early 1970s [*Zhou and Zhang*, 2009]. The atmospheric fields from the reanalyses before the modern satellite era (since 1979) are

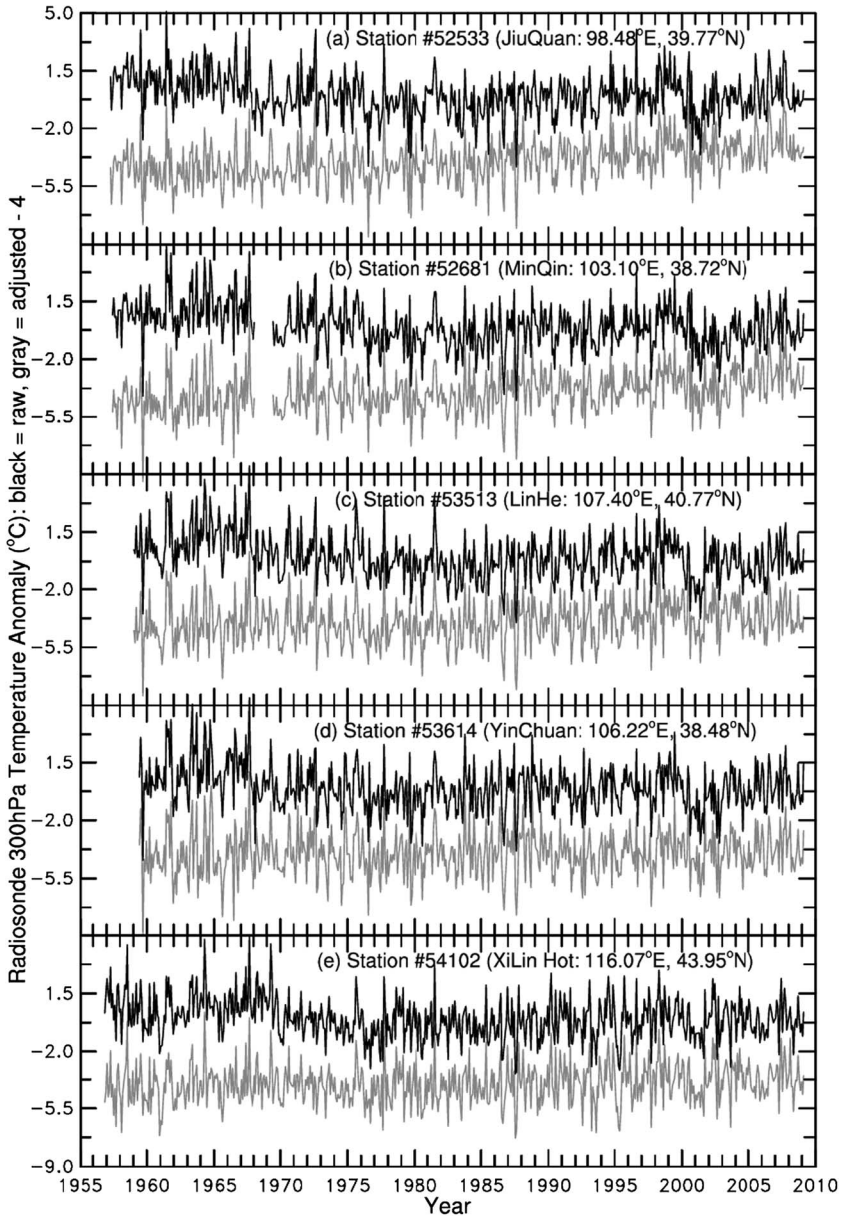

Figure B2. Time series of monthly temperature anomalies at 300 hPa computed using raw (black) and homogenized (gray, shifted downward by 4°C) 00 and 12UTC radiosonde reports at all five stations that have data since the late 1950s and are around the cooling center over East Asia of Figure B1e.There are only three Mongolia stations in the cooling area that had some reports back to around 1966, and their records contain some discontinuities around the late 1960s that may also have contributed to the cooling shown in Figure B1e.

constrained primarily by radiosonde observations from a sparse network over land, as there were no or very few upper-air observations over the oceans before around 1979. Note that surface observations have not been assimilated by most reanalysis systems so far. Figure B2 (black line) shows that the temperature records from all the Chinese radiosonde stations around the cooling center with data back to the 1950s show many stepwise drops at 300 hPa (and other levels, not shown) from the 1950s to the early 1970s. In particular, all the stations exhibit a discontinuity around 1966–1970, which is the peak period of the Cultural Revolution that disrupted most activities within China. An examination of the updated (but still vastly incomplete) metadata from the IGRA website (http://www1.ncdc.noaa.gov/pub/data/igra/igra-metadata.txt) revealed a number of instrumental and observational changes such as those associated with radiation corrections from the 1950s to the early 1970s. Both the NCEP/NCAR and ERA-40 reanalyses used the unhomogenized radiosonde data and had no built-in homogenization procedures to remove the spurious changes. Thus, all the discontinuities shown in Figure B2 (and at other Chinese stations) were assimilated into the reanalysis data and therefore have contributed to the cooling trends seen in the reanalysis data. This was confirmed by the fact that the temperature time series from the NCEP/NCAR and ERA-40 reanalyses (figures not shown) for the collocated boxes containing the stations of Figure B2 show

temporal evolutions similar to the unhomogenized series shown in Figure B2.

[54] Examinations of a few homogenized radiosonde temperature data sets over China [*Guo et al*., 2008; *Guo and Ding*, 2009] still show the tropospheric cooling, albeit at reduced magnitudes. These studies assumed homogeneity of a reference series derived either from the NCEP/NCAR reanalysis data or from unhomogenized radiosonde data from nearby stations. Given that similar discontinuities exist in the reanalysis data and in nearby station records around the cooling center, it is likely that the reference series and thus the homogenized data in these studies contain a significant portion of the discontinuities shown by the black line in Figure B2. Our examination of another homogenized radiosonde temperature data set from *Haimberger et al*. [2008] revealed that most of the inhomogeneities before the early 1970s for the stations shown in Figure B2 still exist in their homogenized data (figure not shown). *Haimberger et al*. [2008] used ERA-40 background forecast temperature fields as the reference series, which is likely affected by the mean biases in the radiosonde data that determine the initial conditions used for the short-term forecast.

[55] Adapting the homogenization approach for daily radiosonde humidity data described by *Dai et al*. [2011], we performed a new homogenization of the Chinese radiosonde daily temperature data using the Kolmogorov-Smirnov (K-S) test to detect abrupt change points and a quantile-matching algorithm to adjust the histograms of the daily temperature data for each segments at each level and each observation time. We used the high-passed NCEP/NCAR reanalysis daily temperature (with variations >1 year time scales being removed) and the 20th century reanalysis (20CR [*Compo et al*., 2011]) daily temperature to remove most natural variations in the radiosonde daily temperature. Unlike other reanalyses, the 20CR was forced only by observed SST and SLP, which are fairly homogeneous since the 1950s (Xiaolan Wang, personal comm. 2011). Thus, it is reasonable to assume that the 20CR data are homogeneous. The results of our homogenization (gray line in Figure B2) suggest that most of the tropospheric cooling from the 1950s to the early 1970s over East Asia may be due to instrumental or observational changes.

[56] The errors in the reanalysis data likely have enhanced the downward trends in the reanalysis thermal contrasts, EASMIu, and EASMIv shown in Figures 8 and 9, especially for the west-east direction, leading to larger trend magnitudes than in the models. A portion of the downward trends in the north-south direction (Figure 8) results from the warming in the tropical troposphere, and this portion is roughly captured by the SST-forced AM2.1 and CAM3 model runs (Figure B1). In the models, the tropical tropospheric warming occurred mainly around the late 1960s, while in both reanalyses it occurred around the middle 1960s (Figure 8). This phase difference may also have resulted from the spurious cooling over East Asia.

[57] Some studies [e.g., *Duan and Wu*, 2008; *Ding et al*., 2009; *Zhao et al*., 2010] have suggested that reduced sensible heating over the TP resulting from increased winter and spring snow cover over the TP since around 1977 may have contributed significantly to the weakening in the land-ocean thermal contrasts and thus in the EASMIu and EASMIv. However, even if the apparent cooling in the reanalysis data is real, it occurred before 1977 (Figures 9 and 10) [*Zhou and Zhang*, 2009], and it is centered to the northeast of the TP with a maximum around 300 hPa (Figure 11) [*Yu and Zhou*, 2007], rather than at the height of the TP (around 700 hPa). Furthermore, a heating change over the TP would have a direct impact on the SASM, yet Figures 10a–b show much weaker trends than those for the EASM (Figures 8 and 9). We therefore conclude that the increased snow cover over the TP since around 1977 is not a major cause for the apparent large decreases in the land-ocean thermal contrasts and the weakening of the EASM seen in reanalysis data, which occurred mostly from the 1950s to the early 1970s (Figures 9 and 10). A large part of this weakening may have resulted from errors in the radiosonde data assimilated into the reanalyses. The remaining part may be real resulting from tropical tropospheric warming (Figure B1).

[58] **Acknowledgments.** Y. Sun was supported by the Chinese 973 program (grant 2012CB417205 and 2010CB428606). C. Chou was supported under Taiwan's National Science Council (grant 99-2111-M-001-003-MY3). The National Center for Atmospheric Research (NCAR) is sponsored by the U.S. National Science Foundation.

References

Bhaskaran, B. (2012), The reversing roles of local and remote circulations on the Indian summer monsoon under a warming scenario, *J. Geophys. Res.*, *117*, D05110, doi:10.1029/2011JD016741.

Chen, H., T. Zhou, R. Neale, X. Wu, and G. J. Zhang (2010), Performance of the new NCAR CAM3.5 in East Asian summer monsoon simulations: Sensitivity to modifications of the convection scheme, *J. Clim.*, *23*, 3657–3675.

Chiang, J. C. H., and A. H. Sobel (2002), Tropical tropospheric temperature variations caused by ENSO and their influence on the remote tropical climate, *J. Clim.*, *15*, 2616–2631.

Chou, C. (2003), Land-sea heating contrast in an idealized Asian summer monsoon, *Clim. Dyn.*, *21*, 11–25.

Chou, C., and J. D. Neelin (2003), Mechanisms limiting the northward extent of the northern summer monsoons over North America, Asia and Africa, *J. Clim.*, *16*, 406–425.

Chou, C., J.-Y. Tu, and J.-Y. Yu (2003), Interannual variability of the western North Pacific summer monsoon: Differences between ENSO and non-ENSO years, *J. Clim.*, *16*, 2275–2287.

Chou, C., J. D. Neelin, C.-A. Chen, and J.-Y. Tu (2009), Evaluating the "rich-get-richer" mechanism in tropical precipitation change under global warming, *J. Clim.*, *22*, 1982–2005.

Compo, G. P., et al. (2011), The twentieth century reanalysis project, *Q. J. R. Meteorol. Soc.*, *137*, 1–28.

Dai, A., T. M. L. Wigley, B. A. Bovilie, J. T. Kiehl, and L. E. Buja (2001), Climates of the twentieth and twenty-first centuries simulated by the NCAR climate system model, *J. Clim.*, *14*, 485–518.

Dai, A., J. Wang, P. W. Thorne, D. E. Parker, L. Haimberger, and X.L. Wang (2011), A new approach to homogenize daily radiosonde humidity data, *J. Climate*, *24*, 965–991.

Ding, Y. H., and J. C. L. Chan (2005), The East Asian summer monsoon: An overview, *Meteorol. Atmos. Phys.*, *89*, 117–142.

Ding, Y. H., Y. Sun, Z. Y. Wang, Y. X. Zhu, and Y. F. Song (2009), Inter-decadal variation of the summer precipitation in China and its association with decreasing Asian summer monsoon. Part II: Possible causes, *Int. J. Climatol.*, *29*, 1926–1944.

Duan, A. M., and G. X. Wu (2005), Role of the Tibetan Plateau thermal forcing in the summer climate patterns over subtropical Asia, *Clim. Dyn.*, *2*, 793–807.

Duan A., and G. X. Wu (2008), Weakening trend in the atmospheric heat source over the Tibetan Plateau during recent decades. Part I: Observations, *J. Climate*, *21*, 3149–3164.

Fu, C. B., and J. O. Fletcher (1985), The relationship between Tibet-tropical ocean thermal contrast and interannual variability of Indian monsoon rainfall, *J. Clim. Appl. Meteorol.*, *24*, 841–847.

Goswami, B. N., and P. K. Xavier (2005), ENSO control on the south Asian monsoon through the length of the rainy season, *Geophys. Res. Lett.*, *32*, L18717, doi:10.1029/2005GL023216.

Guo, Q. Y. (1983), The summer monsoon intensity index in East Asia and its variation [in Chinese], *Acta Geogr. Sin.*, *38*, 207–217.

Guo, Y. J., and Y. H. Ding (2009), Long-term free-atmosphere temperature trends in China derived from homogenized in situ radiosonde temperature series, *J. Climate*, *22*, 1037–1051.

Guo, Y. J., P. W. Thorne, M. P. McCarthy, H. A. Titchner, B. X. Huang, P. M. Zhai, and Y. H. Ding (2008), Radiosonde temperature trends and their uncertainties over eastern China, *Int. J. Climatol.*, *28*, 1269–1281.

Haimberger, L., C. Tavolato, and S. Sperka (2008), Toward elimination of the warm bias in historic radiosonde temperature records — Some new results from a comprehensive intercomparison of upper-air data, *J. Climate*, *21*, 4587–4606.

He, H., C.-H. Sui, M. Jian, Z. Wen, and G. Lan (2003), The evolution of tropospheric temperature field and its relationship with the onset of Asian summer monsoon, *J. Meteorol. Soc. Jpn.*, *81*, 1201–1223.

He, J., J. Yu, X. Shen, and H. Gao (2004), Research on mechanism and variability of East Asian monsoon [in Chinese], *J. Trop. Meteorol.*, *20*, 449–459.

He, J. J., J. H. Ju, Z. P. Wen, J. M. Lu, and Q. H. Jin (2007), A review of recent advances in research on Asian monsoon in China, *Adv. Atmos. Sci.*, *24*, 972–992.

Holton, J. R. (2004), *An Introduction to Dynamic Meteorology*, Int. Geophys. Ser., vol. 88, 4th ed., edited by R. Dmowska, J. R. Holton, and H. T. Rossby, 535 pp., Elsevier Acad., Burlington, Mass.

Kalnay, E., et al. (1996), The NCEP/NCAR 40-year reanalysis project, *Bull. Am. Meteorol. Soc.*, *77*, 437–471.

Kawamura, R. (1998), A possible mechanism of the Asian summer monsoon-ENSO coupling, *J Meteorol. Soc. Jpn.*, *76*, 1009–1027.

Kitoh, A. (2006), Asian monsoons in the future, in *The Asian Monsoon*, edited by B. Wang, pp. 631–649, Springer-Praxis, Chichester, U. K.

Kripalani, R. H., J. H. Oh, A. Kulkarni, S. Sabade, and H. S. Chaudhari (2007a), South Asian summer monsoon precipitation variability: Coupled climate model simulations and projections under IPCC AR4, *Theor. Appl. Climatol.*, *90*, 133–159.

Kripalani, R. H., J. H. Oh, and H. S. Chaudhari (2007b), Response of the East Asian summer monsoon to doubled atmospheric CO2: Coupled climate model simulations and projections under IPCC AR4, *Theor. Appl. Climatol.*, *87*, 1–28.

Kucharski, F., A. Bracco, R. Barimalala, and J. H. Yoo (2011), Contribution of the east-west thermal heating contrast to the South Asian Monsoon and consequences for its variability, *Clim. Dyn.*, *37*, 721–735.

Li, C. F., and Yanai (1996), The onset and interannual variability of the Asian summer monsoon in relation to land-sea thermal contrast, *J. Clim.*, *9*, 358–375.

Li, H., A. Dai, T. Zhou, and J. Lu (2010), Response of East Asian summer monsoon to historical SST and atmospheric forcing during 1950-2000, *Clim. Dyn.*, *34*, 501–514.

Santer, B. D., et al. (2005), Amplification of surface temperature trends and variability in the tropical atmosphere, *Science*, *309*, 1551–1556.

Schneider, E., and R. Lindzen (1977), Axially symmetric steady state models of the basic state of instability and climate studies. Part I: Linearized calculations, *J. Atmos. Sci.*, *34*, 23–279.

Su, H., and J. D. Neelin (2002), Teleconnection mechanisms for tropical Pacific descent anomalies during El Niño, *J. Atmos. Sci.*, *59*, 2682–2700.

Sun, Y., and Y. H. Ding (2010), A projection of future changes in summer precipitation and monsoon in East Asia, *Sci. China Earth Sci.*, *53*, 284–300.

Sun, Y., and Y. H. Ding (2011), Responses of South and East Asian summer monsoons to different land-sea temperature increases under a warming scenario, *Chin. Sci. Bull.*, *56*, 2618–2726.

Sun, Y., Y. H. Ding, and A. G. Dai (2010), Changing links between South Asian summer monsoon circulation and tropospheric land-sea thermal contrasts under a warming scenario, *Geophys. Res. Lett.*, *37*, L02704, doi:10.1029/2009GL041662.

Trenberth, K. E., and L. Smith (2009), Variations in the three dimensional structure of the atmospheric circulation with different flavors of El Niño, *J. Climate*, *22*(11), 2978–2991.

Uppala, S. M., et al. (2005), The ERA-40 re-analysis, *Q. J. R. Metorol. Soc.*, *131*, 2961–3012.

Wang, B., Z. W. Wu, J. P. Li, J. Liu, C. P. Chang, Y. H. Ding, and G. X. Wu (2008), How to measure the strength of the East Asian summer monsoon, *J. Climate*, *21*, 4449–4463.

Webster, P. J. (1987), The elementary monsoon, in *Monsoons*, edited by J. S. Fein and P. L. Stephens, pp. 3–32, John Wiley, New York.

Webster, P. J., and S. Yang (1992), Monsoon and ENSO: Selectively interactive systems, *Q. J. R. Meteorol. Soc.*, *118*, 877–926.

Webster, P., V. Magaña, T. Palmer, J. Shukla, R. Tomas, M. Yanai, and T. Yasunari (1998), Monsoons: Processes, predictability, and the prospects for prediction, *J. Geophys. Res.*, *103*, 14,451–14,510.

Wu, R., J. L. Kinter III, and B. P. Kirtman (2005), Discrepancy of interdecadal changes in the Asian region among the NCEP–NCAR reanalysis, objective analyses, and observations, *J. Climate*, *18*, 3048–3067.

Yanai, M., and C. Li (1994), Mechanism of heating and the boundary layer over the Tibetan Plateau, *Mon. Weather Rev.*, *122*, 305–323.

Yang, M. Z., Y. H. Ding, W. J. Li, H. Q. Mao, and C. X. Huang (2008), The leading mode of Indian Ocean SST and its impacts on Asian summer monsoon, *Acta Meteorol. Sin.*, *22*, 31–41.

Yang, S., W. S. Olson, J. J. Wang, T. L. Bell, E. A. Smith, and C. D. Kummerow (2006), Precipitation and latent heating distributions from satellite passive microwave radiometry. Part II: Evaluation of estimates using independent data, *J. Appl. Meteorol. Clim.*, *45*, 721–739.

Yu, R. C., and T. J. Zhou (2007), Seasonality and three-dimensional structure of the interdecadal change in East Asian monsoon, *J. Climate*, *20*, 5344–5355.

Yu, R. C., B. Wang, and T. J. Zhou (2004), Tropospheric cooling and summer monsoon weakening trend over East Asia, *Geophys. Res. Lett.*, *31*, L22212, doi:10.1029/2004GL021270.

Zeng, Q., and J. Li (2002), Interactions between the Northern and Southern Hemispheric atmospheres and the essence of monsoon [in Chinese], *Chin. J. Atmos. Sci.*, *26*, 433–448.

Zhang, L., and T. Zhou (2012), The interannual variability of summer upper-tropospheric temperature over East Asia, *J. Climate*, *25*, 6539–6553

Zhang, Y., X. Kuang, W. Guo, and T. Zhou (2006), Seasonal evolution of the upper-tropospheric westerly jet core over East Asia, *Geophys. Res. Lett.*, *33*, L11708, doi:10.1029/2006GL026377.

Zhao, P., S. Yang, and R. C. Yu (2010), Long-term changes in rainfall over eastern China and large-scale atmospheric circulation associated with recent global warming, *J. Climate*, *23*, 1544–1562.

Zhou, T. J., and J. Zhang (2009), Harmonious inter-decadal changes of July–August upper tropospheric temperature across the North Atlantic, Eurasian continent, and North Pacific, *Adv. Atmos. Sci.*, *26*(4), 656–665.

Zhou, T., and L. Zou (2010), Understanding the predictability of East Asian summer monsoon from the reproduction of land-sea thermal contrast change in AMIP-type simulation, *J. Climate*, *23*, 6009–6026.

Zhou, T. J., et al. (2009a), Why the Western Pacific subtropical high has extended westward since the late 1970s, *J. Climate*, *22*, 2199–2215.

Zhou, T. J., D. Y. Gong, J. Li, and B. Li (2009b), Detecting and understanding the multi-decadal variability of the East Asian Summer Monsoon — Recent progress and state of affairs, *Meteorol. Z.*, *18*, 455–467.

Zhou, T., et al. (2009c), The CLIVAR C20C Project: Which components of the Asian-Australian Monsoon circulation variations are forced and reproducible?, *Clim. Dyn.*, *33*, 1051–1068, doi:10.1007/s00382-008-0501-8.